



Rivulet flow round a horizontal cylinder subject to a uniform surface shear stress

by

**C. Paterson
S. K. Wilson
B. R. Duffy**

Rivulet flow round a horizontal cylinder subject to a uniform surface shear stress

C. Paterson, S. K. Wilson*, and B. R. Duffy

*Department of Mathematics and Statistics, University of Strathclyde,
26 Richmond Street, Glasgow G1 1XH, UK*

(Dated: 7th June 2013)

Abstract

The steady flow of a slowly varying rivulet with prescribed flux in the azimuthal direction round a large stationary horizontal cylinder subject to a prescribed uniform azimuthal surface shear stress is investigated. In particular, we focus on the case where the volume flux is downwards but the shear stress is upwards, for which there is always a solution corresponding to a rivulet flowing down at least part of one side of the cylinder. We consider both a rivulet with constant non-zero contact angle but slowly varying width (i.e. de-pinned contact lines) and a rivulet with constant width but slowly varying contact angle (i.e. pinned contact lines), and show that they have qualitatively different behaviour. When shear is present, a rivulet with constant non-zero contact angle can never run all the way from the top to the bottom of the cylinder, and so we consider the scenario in which an infinitely wide two-dimensional film of uniform thickness covers part of the upper half of the cylinder and “breaks” into a single rivulet with constant non-zero contact angle. In contrast, a sufficiently narrow rivulet with constant width can run all the way from the top to the bottom of the cylinder, whereas a wide rivulet can do so only if its contact lines de-pin, and so we consider the scenario in which the contact lines of a wide rivulet de-pin on the lower half of the cylinder.

* Author for correspondence. Email: s.k.wilson@strath.ac.uk, Telephone: + 44 (0) 141 548 3820, Fax: + 44 (0) 141 548 3345.

I. INTRODUCTION

Thin-film and/or rivulet flow on the inside or outside of a cylinder subject to a pressure and/or shear stress arising from an external airflow occurs in many practical contexts, such as in falling-film flow over horizontal-tube evaporators found in refrigeration, desalination and petroleum refining processes (see, for example, Ribatski and Jacobi¹), in the flow of oil films inside aeroengines (see, for example, Gorse, Busam, and Dullenkopf² and Farrall et al.³), and in the rain-wind-induced vibrations of the cables of cable-stayed bridges (see, for example, Hikami and Shiraishi⁴ and Robertson et al.⁵).

The pioneering work on two-dimensional thin-film flow on the outside of a stationary horizontal cylinder was performed by Nusselt^{6,7}, and the corresponding analysis of flow on both the outside and the inside of a rotating horizontal cylinder was carried out by Moffatt⁸. Three-dimensional rivulet flow on the outside of a stationary horizontal cylinder was considered by Duffy and Moffatt⁹, who interpreted their solution for the locally unidirectional draining of a gravity-driven rivulet with constant non-zero contact angle on a slowly varying substrate as the flow in the azimuthal direction of a slowly varying rivulet on a large horizontal cylinder. In particular, they found that the rivulet becomes wide with finite thickness near the top of the cylinder and deep with finite width near the bottom of the cylinder. Recently, the present authors (Paterson, Wilson, and Duffy¹⁰) extended the analysis of Duffy and Moffatt⁹ to consider the possible pinning, de-pinning and re-pinning of the rivulet. They considered both a rivulet with constant contact angle but variable width (i.e. de-pinned contact lines) and a rivulet with constant width but variable contact angle (i.e. pinned contact lines). In particular, they found that a rivulet with constant width can flow from the top to the bottom of the cylinder only if it is sufficiently narrow, and that a wider rivulet can do so only if its contact lines de-pin. An aspect of rivulet flow on a rotating horizontal cylinder was considered by Leslie, Wilson, and Duffy¹¹, who studied a “full ring” of fluid with constant non-zero contact angle that extends all the way round the cylinder and, in particular, for flow on the outside of the cylinder, determined the maximum mass of fluid that can be supported against gravity by the rotation of the cylinder in such a full ring.

The present work is concerned with rivulet flow on a stationary horizontal cylinder, but

now subject to an azimuthal surface shear stress due to an external airflow, and so, in addition to the works discussed above, perhaps the most closely related previous study is that by Villegas-Díaz, Power, and Riley¹², who investigated two-dimensional thin-film flow on the inside of a rotating horizontal cylinder subject to a uniform azimuthal surface shear stress. They found that there is a maximum volume flux such that the film covers the entire cylinder and that this maximum flux is four times greater in the case of rotation with no shear stress than in the case of shear stress with no rotation. Discontinuous solutions with shocks (that is, one or more jumps in the film thickness) are possible both when the shear stress and the rotation are in the same or in opposite directions and, in particular, when they are in opposite directions then these shocks can occur anywhere on the cylinder. To gain further insight into the feasibility of these shock solutions in practice, Villegas-Díaz, Power, and Riley¹³ extended the standard lubrication model to include surface tension and higher-order gravity effects, and offered analytical and numerical results to support the claim that these shock solutions are physically relevant. Another closely related study is that by Sullivan, Wilson, and Duffy¹⁴, who used the approach of Duffy and Moffatt⁹ to investigate the flow of a rivulet of perfectly wetting fluid (i.e. a rivulet with zero contact angle) on the lower half of a stationary horizontal cylinder subject to a uniform azimuthal surface shear stress, and found that the rivulet becomes wide and shallow near the middle of the cylinder and deep with finite width near the bottom of the cylinder. There have been several other studies of various two-dimensional thin-film and three-dimensional rivulet flows on non-cylindrical substrates subject to a surface shear stress arising from an external airflow (see, for example, the work by King, Tuck, and Vanden-Broeck¹⁵, Chou and Wu¹⁶, Wilson, Duffy, and Hunt¹⁷, Myers and Charpin¹⁸, Myers, Liang, and Wetton¹⁹, Wilson and Duffy²⁰, Shuaib et al.²¹, Pascal and D'Alessio²², Cuminato et al.²³, Ueno and Farzaneh²⁴, and Sullivan et al.²⁵). In addition, the flow of a rivulet down an inclined channel subject to an airflow that is blowing up the channel has been investigated experimentally by Luo et al.^{26,27}.

In the present work we use the solution for the steady unidirectional flow of a thin rivulet on an inclined planar substrate to investigate the flow in the azimuthal direction of a slowly varying rivulet on the outside of a large stationary horizontal cylinder subject to a prescribed uniform azimuthal surface shear stress. In particular, in the situation in which the shear

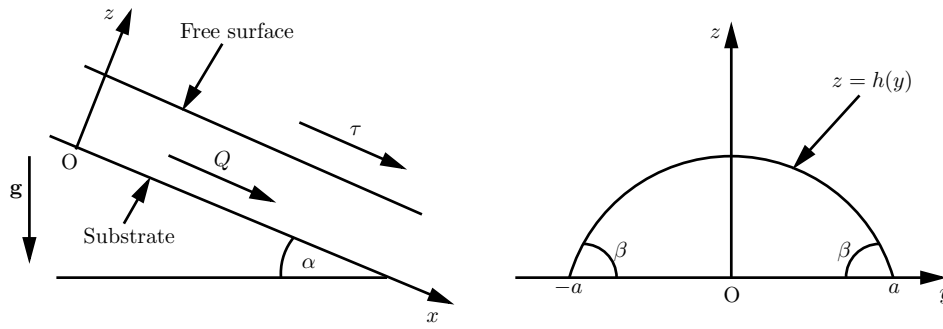


FIG. 1: Sketch of a thin rivulet with semi-width a , contact angle β and volume flux Q flowing on a planar substrate inclined at an angle α to the horizontal subject to a prescribed uniform longitudinal surface shear stress τ .

stress acts in opposition to gravity, we obtain complete descriptions of the flow of a rivulet with constant non-zero contact angle but slowly varying width in which an infinitely wide sheet of fluid covers part of the upper half of the cylinder and “breaks” into a single rivulet, and the flow of a rivulet with constant width but slowly varying contact angle in which the contact lines of a wide rivulet de-pin on the lower half of the cylinder.

II. UNIDIRECTIONAL FLOW ON A PLANAR SUBSTRATE

A. Problem Formulation

Consider the steady unidirectional flow of a thin symmetric rivulet with semi-width a and volume flux Q on a planar substrate inclined at an angle α ($0 \leq \alpha < 2\pi$) to the horizontal subject to a prescribed uniform longitudinal surface shear stress τ . We assume that the fluid is Newtonian with constant viscosity μ , density ρ and coefficient of surface tension γ , and choose Cartesian coordinates $Oxyz$ with the x axis down the line of greatest slope for $0 < \alpha < \pi$ or up the line of greatest slope for $\pi < \alpha < 2\pi$, the y axis horizontal, and the z axis normal to the substrate $z = 0$, such that $\tau > 0$ corresponds to a shear stress in the positive x direction, as sketched in Figure 1. In dimensionless variables the velocity $\mathbf{u} = u(y, z)\mathbf{i}$ and the pressure (relative to its ambient value) $p = p(y, z)$ satisfy the familiar mass-conservation and Navier–Stokes equations subject to the normal stress balance $p = -h''$, the tangential stress balance $u_z = \tau$ and the kinematic condition at the free surface $z = h(y)$, the no-slip condition $u = 0$ at the substrate $z = 0$, and the condition of zero thickness at the contact lines (i.e. $h(\pm a) = 0$), where a dash denotes differentiation with

respect to argument. The contact angle is denoted by $\beta = \mp h'(\pm a) (\geq 0)$ and the maximum thickness of the rivulet, which always occurs at $y = 0$, is denoted by $h_m = h(0)$. We have non-dimensionalised y and a with ℓ , z , h and h_m with $\delta\ell$, u with $U = \delta^2\rho g\ell^2/\mu$, Q with $\delta\ell^2 U = \delta^3\rho g\ell^4/\mu$, p with $\delta\rho g\ell$, and τ with $\delta^2\rho g\ell$, where g is the magnitude of gravitational acceleration, $\ell = (\gamma/\rho g)^{1/2}$ is the capillary length, and δ is the transverse aspect ratio. There is some freedom regarding the definition of δ ; however, for the moment we leave δ unspecified in order to keep the subsequent presentation as general as possible. At leading order in the limit of small transverse aspect ratio $\delta \rightarrow 0$ (i.e. for a thin rivulet) the governing equations are readily solved to yield the pressure

$$p = \cos\alpha(h - z) - h'' \quad (1)$$

and the velocity

$$u = \frac{\sin\alpha}{2}(2h - z)z + \tau z, \quad (2)$$

so that the local flux $\bar{u} = \bar{u}(y)$ is given by

$$\bar{u} = \int_0^h u \, dz = \frac{\sin\alpha}{3}h^3 + \frac{\tau}{2}h^2. \quad (3)$$

We may differentiate (1) with respect to y and use the fact that $p_y = 0$ to obtain a third order ordinary differential equation for the free surface, namely

$$(h \cos\alpha - h'')' = 0, \quad (4)$$

which is to be solved subject to the contact-line conditions $h(\pm a) = 0$ and $\mp h'(\pm a) = \beta (\geq 0)$.

B. The General Case of Non-Zero Contact Angle $\beta > 0$

In the general case of non-zero contact angle $\beta > 0$ we may solve (4) subject to the contact-line conditions to obtain the free surface shape

$$h = \beta \times \begin{cases} \frac{\cosh ma - \cosh my}{m \sinh ma} & \text{for } 0 \leq \alpha < \frac{\pi}{2}, \frac{3\pi}{2} < \alpha < 2\pi, \\ \frac{a^2 - y^2}{2a} & \text{for } \alpha = \frac{\pi}{2}, \frac{3\pi}{2}, \\ \frac{\cos my - \cos ma}{m \sin ma} & \text{for } \frac{\pi}{2} < \alpha < \frac{3\pi}{2}, \end{cases} \quad (5)$$

so that the maximum thickness of the rivulet is given by

$$h_m = \frac{\beta}{m} \times \begin{cases} \tanh\left(\frac{ma}{2}\right) & \text{for } 0 \leq \alpha < \frac{\pi}{2}, \frac{3\pi}{2} < \alpha < 2\pi, \\ \frac{ma}{2} & \text{for } \alpha = \frac{\pi}{2}, \frac{3\pi}{2}, \\ \tan\left(\frac{ma}{2}\right) & \text{for } \frac{\pi}{2} < \alpha < \frac{3\pi}{2}, \end{cases} \quad (6)$$

and the volume flux is given by

$$Q = \int_{-a}^a \bar{u} dy = \frac{\beta^3 \sin \alpha}{9m^4} f(ma) + \frac{\beta^2 \tau}{2m^3} g(ma), \quad (7)$$

where we have written $m = |\cos \alpha|^{1/2}$. The functions $f = f(ma)$ and $g = g(ma)$ appearing in (7) are defined by

$$f(ma) = \begin{cases} 15ma \coth^3 ma - 15 \coth^2 ma - 9ma \coth ma + 4 & \text{for } 0 \leq \alpha < \frac{\pi}{2}, \frac{3\pi}{2} < \alpha < 2\pi, \\ \frac{12}{35}(ma)^4 & \text{for } \alpha = \frac{\pi}{2}, \frac{3\pi}{2}, \\ -15ma \cot^3 ma + 15 \cot^2 ma - 9ma \cot ma + 4 & \text{for } \frac{\pi}{2} < \alpha < \frac{3\pi}{2} \end{cases} \quad (8)$$

and

$$g(ma) = \begin{cases} 3ma \coth^2 ma - 3 \coth ma - ma & \text{for } 0 \leq \alpha < \frac{\pi}{2}, \frac{3\pi}{2} < \alpha < 2\pi, \\ \frac{4}{15}(ma)^3 & \text{for } \alpha = \frac{\pi}{2}, \frac{3\pi}{2}, \\ 3ma \cot^2 ma - 3 \cot ma + ma & \text{for } \frac{\pi}{2} < \alpha < \frac{3\pi}{2}. \end{cases} \quad (9)$$

Note that the function $f(ma)$ was first obtained by Duffy and Moffatt⁹ (their equation (14) and denoted as $F(B)$) and the function $g(ma)$ was first obtained by Sullivan, Wilson, and Duffy¹⁴ (their equation (2.16)). For $0 \leq \alpha < \pi/2$ and $3\pi/2 < \alpha < 2\pi$ both f and g are positive, monotonically increasing functions, increasing from zero at $ma = 0$ to infinity as $ma \rightarrow \infty$, while their derivatives f' and g' are also positive, monotonically increasing functions, increasing from zero at $ma = 0$ to 6 and 2, respectively, as $ma \rightarrow \infty$. Figure 2(a) shows plots of f , g , f' , and g' as functions of ma for $0 \leq \alpha < \pi/2$ and $3\pi/2 < \alpha < 2\pi$. For $\pi/2 < \alpha < 3\pi/2$ both f and g have multiple branches, but we restrict our attention to the branches in the interval $0 \leq ma < \pi$ since these are the only ones for which the solution is physically realisable (specifically, for which $h \geq 0$ everywhere in the interval $y = -a$

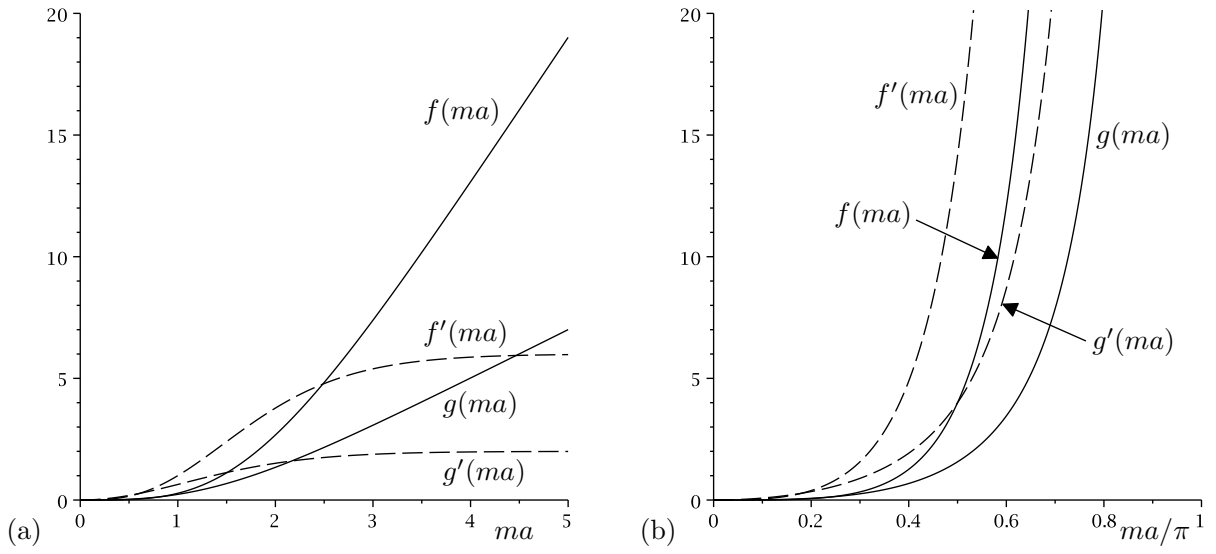


FIG. 2: Plots of f and g (solid lines), defined by (8) and (9), respectively, together with their derivatives f' and g' (dashed lines) as (a) functions of ma for $0 \leq \alpha < \pi/2$ and $3\pi/2 < \alpha < 2\pi$ when $0 \leq ma < \infty$, and (b) functions of ma/π for $\pi/2 < \alpha < 3\pi/2$ when $0 \leq ma < \pi$.

to $y = +a$). Then f and g and their derivatives f' and g' are all positive, monotonically increasing functions, increasing from zero at $ma = 0$ to infinity as $ma \rightarrow \pi^-$. Figure 2(b) shows plots of f , g , f' , and g' as functions of ma/π for $\pi/2 < \alpha < 3\pi/2$. For future reference it is useful to note that in the limit $ma \rightarrow 0^+$

$$f(ma) = \begin{cases} \frac{12}{35}(ma)^4 - \frac{8}{105}(ma)^6 + O(ma)^8 & \text{for } 0 \leq \alpha < \frac{\pi}{2}, \frac{3\pi}{2} < \alpha < 2\pi, \\ \frac{12}{35}(ma)^4 + \frac{8}{105}(ma)^6 + O(ma)^8 & \text{for } \frac{\pi}{2} < \alpha < \frac{3\pi}{2} \end{cases} \quad (10)$$

and

$$g(ma) = \begin{cases} \frac{4}{15}(ma)^3 - \frac{4}{105}(ma)^5 + O(ma)^7 & \text{for } 0 \leq \alpha < \frac{\pi}{2}, \frac{3\pi}{2} < \alpha < 2\pi, \\ \frac{4}{15}(ma)^3 + \frac{4}{105}(ma)^5 + O(ma)^7 & \text{for } \frac{\pi}{2} < \alpha < \frac{3\pi}{2}. \end{cases} \quad (11)$$

In the limit $ma \rightarrow \infty$ for $0 \leq \alpha < \pi/2$ and $3\pi/2 < \alpha < 2\pi$

$$f(ma) = 6ma - 11 + O(ma \exp(-2ma)) \quad (12)$$

and

$$g(ma) = 2ma - 3 + O(ma \exp(-2ma)). \quad (13)$$

In the limit $ma \rightarrow \pi^-$ for $\pi/2 < \alpha < 3\pi/2$

$$f(ma) = \frac{15\pi}{(\pi - ma)^3} + O(\pi - ma)^{-1} \quad (14)$$

and

$$g(ma) = \frac{3\pi}{(\pi - ma)^2} + O(1). \quad (15)$$

C. The Special Case of Zero Contact Angle $\beta = 0$

In the special case of zero contact angle $\beta = 0$ we recover the solution for a rivulet of perfectly wetting fluid analysed by Sullivan, Wilson, and Duffy¹⁴, namely that there is no solution for $0 \leq \alpha \leq \pi/2$ and $3\pi/2 \leq \alpha < 2\pi$, but

$$a = \frac{\pi}{m}, \quad h = \frac{h_m}{2} (1 + \cos my), \quad Q = \frac{\pi}{24m} (5 \sin \alpha h_m + 9\tau) h_m^2 \quad \text{for} \quad \frac{\pi}{2} < \alpha < \frac{3\pi}{2}. \quad (16)$$

D. Cross-Sectional Flow Patterns

All of the possible cross-sectional flow patterns that can occur within the rivulet may be categorised into five types which, following the notation used by Wilson and Duffy²⁰ and Sullivan, Wilson, and Duffy¹⁴, we denote as type I to type V. The flow patterns for a rivulet on a substrate inclined at an angle α for $0 < \alpha < \pi$ with shear stress τ and volume flux Q are equivalent to those for $\pi < \alpha < 2\pi$ with shear stress $-\tau$ and volume flux $-Q$, and hence, without loss of generality, in the rest of this subsection we restrict our attention to the interval $0 < \alpha < \pi$.

Figure 3 shows sketches of these five different types of flow pattern when $\beta > 0$ at $\alpha = \pi/2$, for which the rivulet has a parabolic profile. Regions with $u > 0$ (i.e. downwards flow for $0 < \alpha < \pi$) are shaded and regions with $u < 0$ are unshaded. When $\beta = 0$ and/or $\alpha \neq \pi/2$ the rivulet profile is not parabolic; however, the flow patterns in these cases are qualitatively the same as those shown in Figure 3. The locations of the maximum and minimum velocities are marked with dots, and expressions for these points for each flow type are the same as those given by Sullivan, Wilson, and Duffy¹⁴ and hence are not reproduced here for brevity. When $\tau > 0$ the shear stress acts down the substrate in co-operation with gravity and so the velocity is downwards throughout the rivulet (type-I flow), but when $\tau < 0$ the shear stress acts up the substrate in opposition to gravity, and the velocity is always upwards near the contact lines (types-II–V flow). The velocity within the rivulet is zero on the curve $z = 2(h - \tau/\sin \alpha)$; with $z = h = h_m$ this shows, in particular, that type-III flow occurs

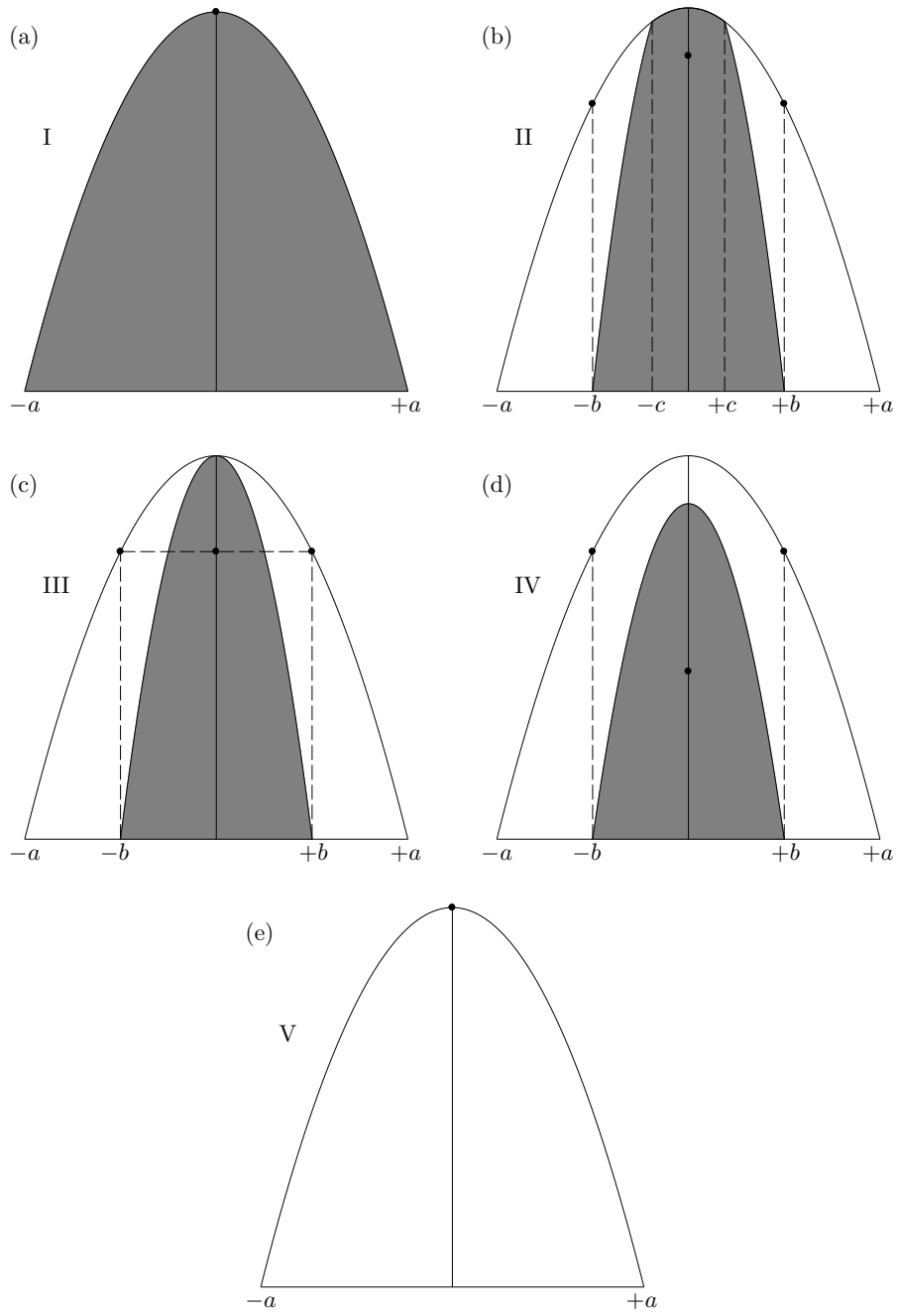


FIG. 3: Sketches of the five different types of cross-sectional flow pattern, denoted as type I to type V, when $\beta > 0$ at $\alpha = \pi/2$, for which the rivulet has a parabolic profile. Regions with $u > 0$ (i.e. downwards flow for $0 < \alpha < \pi$) are shaded and regions with $u < 0$ are unshaded. The locations of the maximum and minimum velocities are marked with dots. When $\beta = 0$ and/or $\alpha \neq \pi/2$ the rivulet profile is not parabolic; however, the flow patterns in these cases are qualitatively the same as those shown here.

when $h_m = -2\tau/\sin\alpha$. For flow types II–IV this curve of zero velocity meets the substrate when $y = \pm b$, and for flow type II it meets the free surface when $y = \pm c$, where b is given

by

$$b = \begin{cases} \frac{1}{m} \cosh^{-1} \left[\cosh ma + \frac{\tau m \sinh ma}{\beta \sin \alpha} \right] & \text{for } 0 < \alpha < \frac{\pi}{2}, \\ \left(a^2 + \frac{2\tau a}{\beta} \right)^{\frac{1}{2}} & \text{for } \alpha = \frac{\pi}{2}, \\ \frac{1}{m} \cos^{-1} \left[\cos ma - \frac{\tau m \sin ma}{\beta \sin \alpha} \right] & \text{for } \frac{\pi}{2} < \alpha < \pi, \end{cases} \quad (17)$$

and c is given by (17) with τ replaced by 2τ .

III. LOCALLY UNIDIRECTIONAL FLOW ROUND A HORIZONTAL CYLINDER

In the remainder of the present work we use the steady unidirectional flow solutions (5)–(9) and (16) to describe the steady, locally unidirectional flow of a slowly varying rivulet with prescribed flux $Q = \bar{Q}$ on a slowly varying substrate, specifically the flow in the azimuthal direction round a large stationary horizontal cylinder, subject to a prescribed uniform azimuthal surface shear stress τ . Note that here and henceforth “slowly varying” means that the longitudinal aspect ratio $\epsilon = \ell/R$, where R is the radius of the cylinder, satisfies $\epsilon \ll \delta$, so that $\epsilon/\delta \rightarrow 0$ in the limit $\epsilon \rightarrow 0$. The angle α is now interpreted as the local slope of the cylinder, with $\alpha = 0$ at the top, increasing down the right-hand side to $\alpha = \pi$ at the bottom, and up the left-hand side to $\alpha = 2\pi$ at the top again. Since a solution with shear stress τ and volume flux \bar{Q} on one side of the cylinder is equivalent to a solution with shear stress $-\tau$ and volume flux $-\bar{Q}$ on the other side, in the remainder of the present work we will, without loss of generality, restrict our attention to the case of positive prescribed flux, $\bar{Q} > 0$ (corresponding to a clockwise flux in the figures shown later).

In practice, when a rivulet flows round a cylinder it is possible that either its contact lines are de-pinned and free to move such that its contact angle remains constant but its width varies, or its contact lines are pinned such that its width remains constant but its contact angle varies. We will therefore consider both of these scenarios in the present work and, in particular, we will show that they have qualitatively different behaviour. Firstly, in Sec. IV we describe a rivulet with constant non-zero contact angle $\beta = \bar{\beta} > 0$ but slowly varying semi-width $a = a(\alpha)$. Imposing the condition of prescribed flux $Q = \bar{Q}$ means that

(7) is a transcendental equation for a which is solved asymptotically in various physically relevant limits and numerically. Secondly, in Sec. V we describe a rivulet with constant semi-width $a = \bar{a}$ but slowly varying contact angle $\beta = \beta(\alpha) (\geq 0)$. Imposing the condition of prescribed flux $Q = \bar{Q}$ means that (7) is a cubic polynomial equation for β which may be solved exactly. We analyse this solution and, in particular, explore its behaviour in various physically relevant limits.

Figure 4 shows a representative selection of rivulet solutions for various values of τ plotted as functions of the scaled angle α/π ($0 \leq \alpha < 2\pi$) when $Q = \bar{Q} = 1$. Expressed in another way, Figure 4 shows contours of the expression for the shear stress τ given by (7) in the α/π – a , α/π – β and α/π – h_m planes, as appropriate, when $Q = \bar{Q} = 1$. Specifically, Figures 4(a) and 4(b) show the semi-width a and maximum thickness h_m for a rivulet with constant non-zero contact angle $\beta = \bar{\beta} = 1$, Figures 4(c) and 4(d) show the contact angle β and maximum thickness h_m for a “narrow” rivulet with constant semi-width $a = \bar{a} = 2 (< \pi)$, and Figures 4(e) and 4(f) show the contact angle β and maximum thickness h_m for a “wide” rivulet with constant semi-width $a = \bar{a} = 5 (> \pi)$, all plotted as functions of α/π for various values of τ . In particular, Figure 4 shows that neither in the case of constant non-zero contact angle nor in the case of constant width does the rivulet have top-to-bottom symmetry (i.e. symmetry about $\alpha = \pi/2$ and $\alpha = 3\pi/2$). As Figure 4 shows, there are various kinds of rivulet solution, some of which exist only in a restricted range of values of α . In particular, in Figures 4(a) and 4(b) there is no physically realisable rivulet solution with $\beta = \bar{\beta} = 1$ when $\tau = -0.5$ in the interval $0 \leq \alpha \leq \alpha_\infty$, where $\alpha_\infty/\pi \simeq 0.2264$. This behaviour (which occurs for all $\tau < 0$) will be discussed in greater detail in Sec. IV, where it will be interpreted as the presence of an infinitely wide sheet of fluid. Similarly, in Figures 4(e) and 4(f) there are no physically realisable rivulet solutions with $a = \bar{a} = 5$ for all values of τ shown in the interval $\alpha_{\text{depin}} < \alpha < 2\pi - \alpha_{\text{depin}}$, where $\alpha_{\text{depin}}/\pi \simeq 0.6292$ and $2 - \alpha_{\text{depin}}/\pi \simeq 1.3708$. This behaviour (which occurs for all values of τ when $\bar{a} > \pi$) will be discussed in greater detail in Sec. V, where it will be interpreted as the occurrence of contact-line de-pinning. Comparison of Figures 4(c) and 4(d) with Figures 4(e) and 4(f) shows that, just as Paterson, Wilson, and Duffy¹⁰ recently found in the special case of no shear stress, $\tau = 0$, unlike a rivulet with constant non-zero contact angle, a “narrow” rivulet with constant semi-width

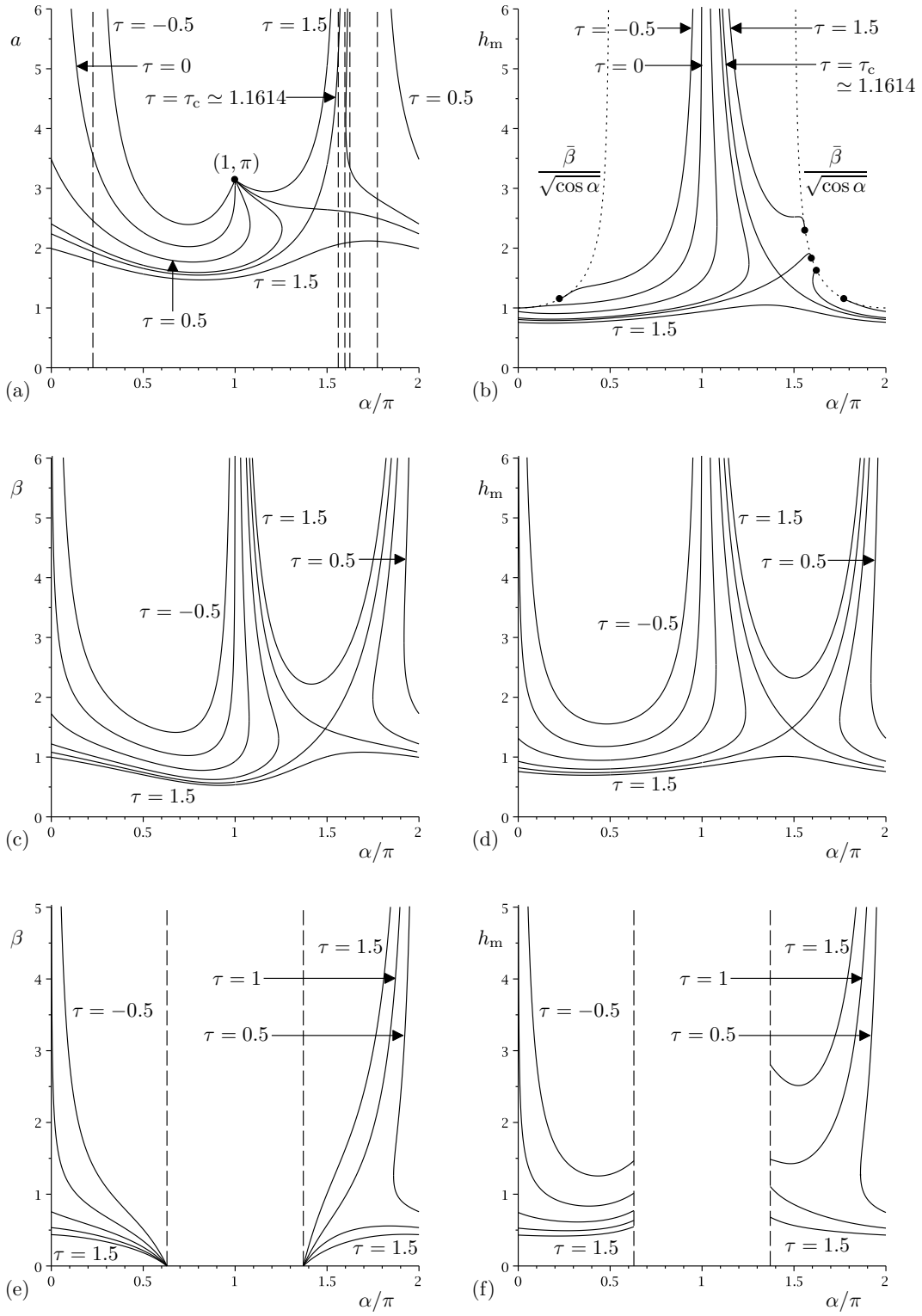


FIG. 4: Plots of (a) the semi-width a , (c,e) the contact angle β , and (b,d,f) the maximum thickness h_m as functions of α/π ($0 \leq \alpha < 2\pi$) when $Q = \bar{Q} = 1$ for (a,b) $\tau = -0.5, 0, 0.5, 1, \tau_c \simeq 1.1614, 1.5$ for a rivulet with constant contact angle $\beta = \bar{\beta} = 1$, (c,d) $\tau = -0.5, 0, 0.5, 1, \tau_c \simeq 1.2741, 1.5$ for a “narrow” rivulet with constant semi-width $a = \bar{a} = 2 (< \pi)$, and (e,f) $\tau = -0.5, 0, 0.5, 1, 1.5$ for a “wide” rivulet with constant semi-width $a = \bar{a} = 5 (> \pi)$. In (a) the vertical dashed lines indicate the values of α/π at which $a \rightarrow \infty$, and in (b) the dots denote the corresponding values of h_m which lie on the curves $h_m = \bar{\beta}/\sqrt{\cos \alpha}$ for $0 \leq \alpha < \pi/2$ and $3\pi/2 < \alpha < 2\pi$, which are denoted with dotted lines. In (e) and (f) the vertical dashed lines correspond to the values of α/π at which $\beta = 0$, namely $\alpha/\pi = \alpha_{\text{depin}}/\pi \simeq 0.6292$ and $\alpha/\pi = 2 - \alpha_{\text{depin}}/\pi \simeq 1.3708$.

$a = \bar{a} < \pi$ behaves qualitatively differently from a “wide” rivulet with constant semi-width $a = \bar{a} > \pi$. Figure 4 also shows the existence of a positive critical shear stress, $\tau_c (> 0)$, such that “full-ring” solutions (i.e. solutions for which a , β and h_m are continuous, finite and non-negative for all $0 \leq \alpha < 2\pi$ and $-a \leq y \leq a$), analogous to those studied by Leslie, Wilson, and Duffy¹¹ in the case of flow on a rotating cylinder in the absence of surface shear stress, exist when $\tau \geq \tau_c$ but not when $\tau < \tau_c$.

In the remainder of the present work we focus on just one of the kinds of solution shown in Figure 4, namely the case of non-positive shear stress, $\tau \leq 0$, in which there is always a solution corresponding to a rivulet flowing down at least part of the right-hand side of the cylinder (where the shear stress acts in opposition to gravity, but it is still possible to sustain a positive flux), but never any solutions corresponding to flow on the left-hand side of the cylinder (where the shear stress acts in co-operation with gravity, making it impossible to sustain a positive flux).

IV. A RIVULET WITH CONSTANT NON-ZERO CONTACT ANGLE $\beta = \bar{\beta} > 0$

In this section we describe the steady, locally unidirectional flow of a slowly varying rivulet with constant non-zero contact angle $\beta = \bar{\beta} > 0$ but slowly varying semi-width $a = a(\alpha)$ on the right-hand side of a large horizontal cylinder subject to a non-positive uniform azimuthal surface shear stress $\tau (\leq 0)$ acting in opposition to gravity.

In the special case of no shear, $\tau = 0$, the rivulet becomes infinitely wide at the top of the cylinder (i.e. $a \rightarrow \infty$ as $\alpha \rightarrow 0^+$) and it runs all the way from the top $\alpha = 0$ to the bottom $\alpha = \pi$ of the cylinder; however, as we saw in Figure 4(a), in the general case of strictly negative shear, $\tau < 0$, the rivulet becomes infinitely wide at the station $\alpha = \alpha_\infty$ away from the top of the cylinder (i.e. $a \rightarrow \infty$ as $\alpha \rightarrow \alpha_\infty^+$) and there is no physically realisable rivulet solution in the interval $0 \leq \alpha \leq \alpha_\infty$. The value of α_∞ ($0 \leq \alpha_\infty < \pi/2$) is determined by the leading order balance in (7) when $a \rightarrow \infty$, namely

$$2\bar{\beta} \sin \alpha + 3m\tau = 0 \tag{18}$$

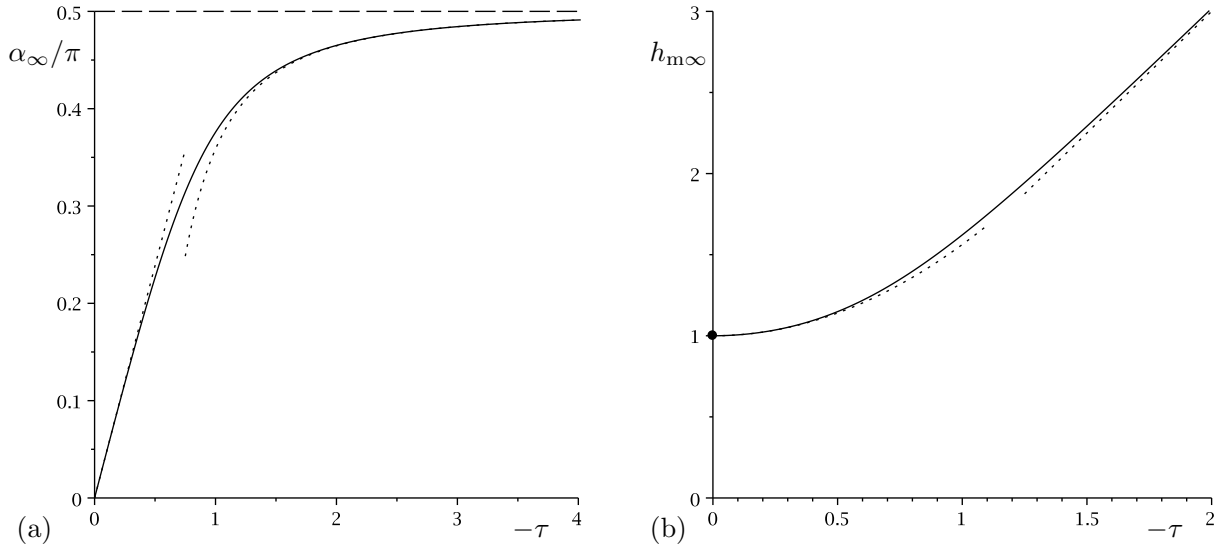


FIG. 5: Plots of (a) the scaled azimuthal angle at which the rivulet becomes infinitely wide, α_∞/π , given by (19), and (b) the corresponding maximum thickness, $h_{m\infty}$, given by (20), as functions of $-\tau$ (≥ 0) when $\bar{\beta} = 1$. The dotted curves show the asymptotic results in the limits of weak shear, $-\tau \rightarrow 0^+$, and strong shear, $-\tau \rightarrow \infty$, given by (21) and (22), respectively.

evaluated at $\alpha = \alpha_\infty$, and is therefore given by

$$\alpha_\infty = \cos^{-1} \left(\frac{\sqrt{81\tau^4 + 64\bar{\beta}^4} - 9\tau^2}{8\bar{\beta}^2} \right), \quad (19)$$

while the corresponding value of the maximum thickness $h_m = h_{m\infty}$ is given by

$$h_{m\infty} = \frac{\bar{\beta}}{\sqrt{\cos \alpha_\infty}} = \frac{\left[\sqrt{81\tau^4 + 64\bar{\beta}^4} + 9\tau^2 \right]^{\frac{1}{2}}}{2\sqrt{2}}. \quad (20)$$

Figure 5 shows plots of α_∞/π and $h_{m\infty}$ as functions of $-\tau$ (≥ 0) when $\bar{\beta} = 1$, and shows that both α_∞ and $h_{m\infty}$ are monotonically increasing functions of $-\tau$. In particular, in the limit of weak shear, $\tau \rightarrow 0^-$, the rivulet becomes infinitely wide near the top of the cylinder and correspondingly its maximum thickness approaches the finite value $\bar{\beta}$ from above according to

$$\alpha_\infty \sim -\frac{3\tau}{2\bar{\beta}} \rightarrow 0^+ \quad \text{and} \quad h_{m\infty} \sim \bar{\beta} + \frac{9\tau^2}{16\bar{\beta}} \rightarrow \bar{\beta}^+, \quad (21)$$

while in the limit of strong shear, $\tau \rightarrow -\infty$, the rivulet becomes infinitely wide near the middle of the cylinder and correspondingly its maximum thickness becomes infinite according to

$$\alpha_\infty \sim \frac{\pi}{2} - \frac{4\bar{\beta}^2}{9\tau^2} \rightarrow \frac{\pi}{2}^- \quad \text{and} \quad h_{m\infty} \sim -\frac{3\tau}{2} \rightarrow \infty. \quad (22)$$

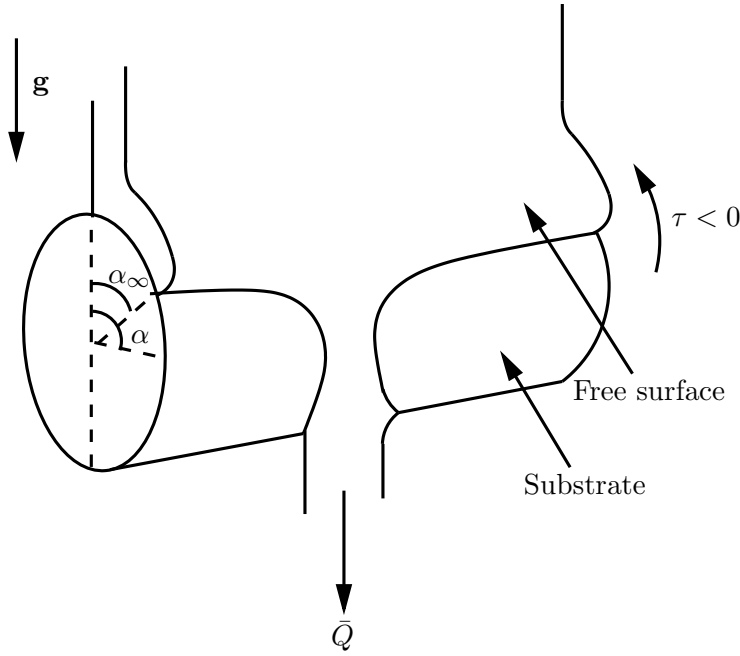


FIG. 6: Sketch of the scenario considered in Sec. IV, namely an infinitely wide two-dimensional film of uniform thickness $H = H(\alpha)$ covers the cylinder from $\alpha = 0$ to $\alpha = \alpha_\infty$, where it “breaks” into a single rivulet with prescribed flux $Q = \bar{Q}$, constant contact angle $\beta = \bar{\beta} (> 0)$ and slowly varying semi-width a that runs from $\alpha = \alpha_\infty$ to $\alpha = \pi$.

Since there is no physically realisable rivulet solution in the interval $0 \leq \alpha \leq \alpha_\infty$, an alternative description of the behaviour is required there. Perhaps the most natural scenario is that an infinitely wide two-dimensional film of uniform thickness $H = H(\alpha)$ covers the cylinder from $\alpha = 0$ to $\alpha = \alpha_\infty$, where it “breaks” into a single rivulet with prescribed flux $Q = \bar{Q}$ that runs from $\alpha = \alpha_\infty$ to the bottom of the cylinder $\alpha = \pi$. This scenario is sketched in Figure 6 and is the one that we will consider here. The appropriate form of H , determined by setting $\bar{u} = 0$ and $h = H$ in (3), is

$$H = -\frac{3\tau}{2\sin\alpha} (> 0). \quad (23)$$

In particular, (23) shows that the film becomes deep near the top of the cylinder according to

$$H \sim -\frac{3\tau}{2\alpha} \rightarrow \infty \quad (24)$$

as $\alpha \rightarrow 0^+$, and that it approaches the finite thickness $h_{\text{m}\infty}$ from above according to

$$H \sim h_{\text{m}\infty} - \frac{2\bar{\beta}^2}{3\tau} (\alpha_\infty - \alpha) \rightarrow h_{\text{m}\infty}^+ \quad (25)$$

as $\alpha \rightarrow \alpha_\infty^-$. Similarly, (7) shows that the rivulet becomes infinitely wide according to

$$a \sim \frac{4 \left[3(\cos \alpha_\infty)^{\frac{3}{2}} \bar{Q} - \bar{\beta}^2 \tau \right]}{\bar{\beta} \sqrt{81\tau^4 + 64\bar{\beta}^4} (\alpha - \alpha_\infty)} \rightarrow \infty \quad (26)$$

and (6) shows that it approaches the finite maximum thickness $h_{m\infty}$ from above according to

$$h_m \sim h_{m\infty} + \frac{h_{m\infty} \tan \alpha_\infty}{2} (\alpha - \alpha_\infty) \rightarrow h_{m\infty}^+ \quad (27)$$

as $\alpha \rightarrow \alpha_\infty^+$, so that the infinitely wide film in $0 \leq \alpha \leq \alpha_\infty$ and the finite-width rivulet in $\alpha_\infty < \alpha \leq \pi$ join continuously (but not smoothly) at the station $\alpha = \alpha_\infty$. In the special case of no shear, $\tau = 0$, the rivulet becomes deep with finite semi-width π near the bottom of the cylinder according to

$$a \sim \pi - \left(\frac{5\bar{\beta}^3(\pi - \alpha)}{3\bar{Q}} \right)^{\frac{1}{3}} \rightarrow \pi^- \quad \text{and} \quad h_m \sim \left(\frac{24\bar{Q}}{5(\pi - \alpha)} \right)^{\frac{1}{3}} \rightarrow \infty \quad (28)$$

as $\alpha \rightarrow \pi^-$, while in the general case of strictly negative shear, $\tau < 0$, the rivulet again becomes deep with finite semi-width π near the bottom of the cylinder, but now according to

$$a \sim \pi + \frac{10\bar{\beta}(\pi - \alpha)}{9\tau} \rightarrow \pi^- \quad \text{and} \quad h_m \sim -\frac{9\tau}{5(\pi - \alpha)} \rightarrow \infty \quad (29)$$

as $\alpha \rightarrow \pi^-$.

The behaviour of the present solution is illustrated in Figure 7, which shows plots of the semi-width a and the maximum thickness h_m as functions of α/π when $\bar{\beta} = 1$ for (a,b) various values of $\tau (\leq 0)$ when $\bar{Q} = 1$ and for (c,d) various values of \bar{Q} when $\tau = -0.5$.

In Subsec. IV A we present examples of free surface profiles of the film and the rivulet, and in Subsecs IV B–IV E we describe the behaviour in the limits of weak shear, $\tau \rightarrow 0^-$, strong shear, $\tau \rightarrow -\infty$, small flux, $\bar{Q} \rightarrow 0^+$, and large flux, $\bar{Q} \rightarrow \infty$, respectively.

A. Free Surface Profiles

Figure 8 shows examples of cross-sectional free-surface profiles of the film and the rivulet in the case $\bar{\beta} = 1$, $\tau = -0.5$ and $\bar{Q} = 1$. For these parameter values we obtain $\alpha_\infty \simeq 0.7112$, and so the profile shown for $\alpha = \pi/8 < \alpha_\infty \simeq 0.7112$ is simply a horizontal line that corresponds to an infinitely wide film of uniform thickness $H \simeq 1.9598$.

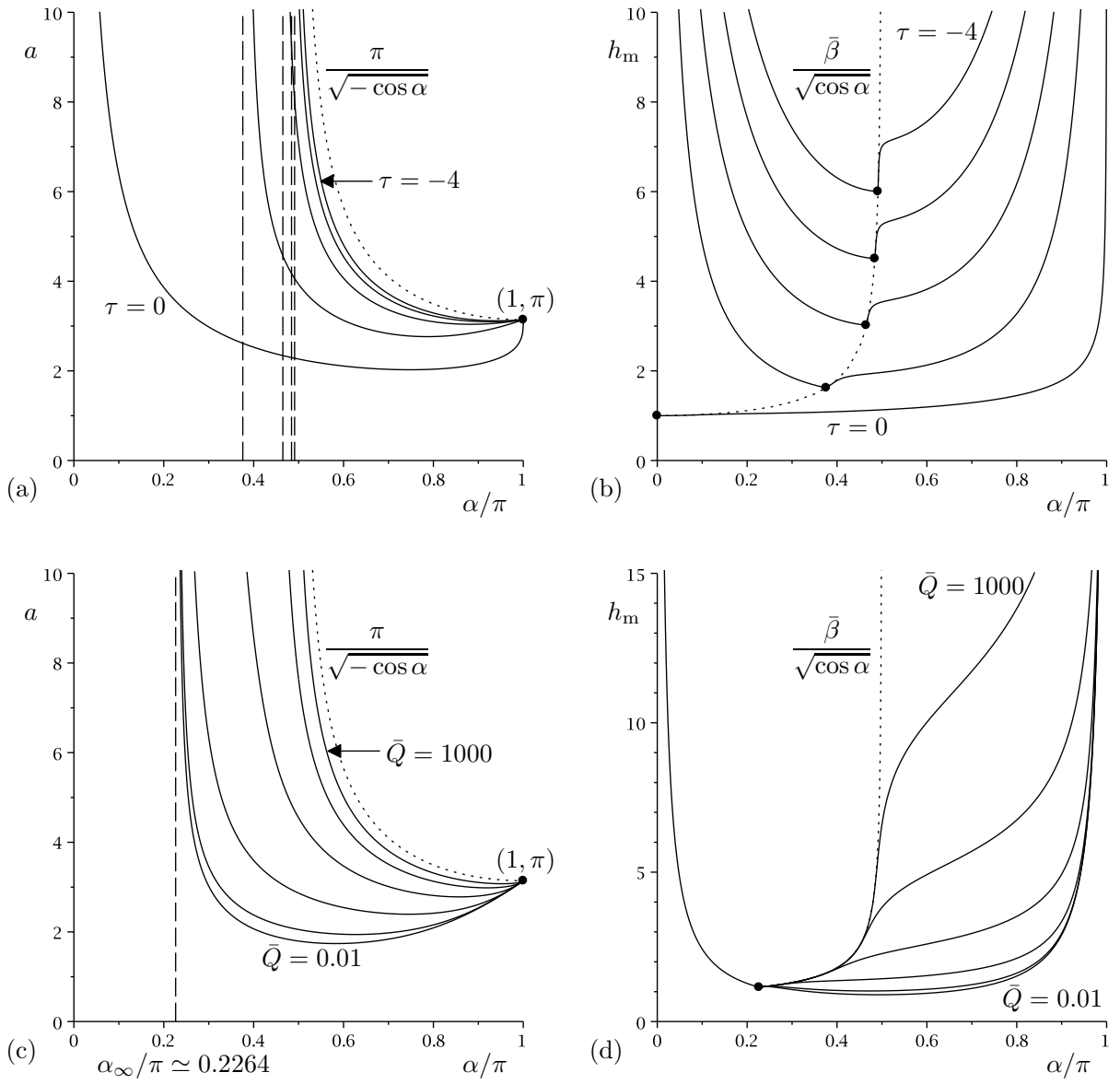


FIG. 7: Plots of (a,c) the semi-width a and (b,d) the maximum thickness h_m as functions of the scaled angle α/π when $\bar{\beta} = 1$ for (a,b) $\tau = -4, -3, \dots, 0$ when $\bar{Q} = 1$ and (c,d) $\bar{Q} = 0.01, 0.1, \dots, 1000$ when $\tau = -0.5$. In (a) and (c) the vertical dashed lines indicate the values of $\alpha/\pi = \alpha_\infty/\pi$, given by (19), at which $a \rightarrow \infty$, and in (b) and (d) the dots denote the corresponding values of h_m which lie on the curve $h_m = \bar{\beta}/\sqrt{\cos \alpha}$ for $0 \leq \alpha < \pi/2$, which is denoted with a dotted line. In (a) and (c) the dotted lines denote the solution $a = \pi/\sqrt{-\cos \alpha}$ for $\pi/2 < \alpha \leq \pi$ attained at leading order in the asymptotic limits $\tau \rightarrow -\infty$ and $\bar{Q} \rightarrow \infty$, respectively.

B. The Limit of Weak Shear ($\tau \rightarrow 0^-$)

In the limit of weak shear, $\tau \rightarrow 0^-$, $\alpha_\infty \rightarrow 0^+$ according to (21) and the rivulet behaves according to

$$a \sim a_{\tau 0} - \frac{9g(ma_{\tau 0})\tau}{2\bar{\beta}\sin \alpha f'(ma_{\tau 0})} \rightarrow a_{\tau 0}^+ \quad \text{and} \quad h_m \sim \frac{\bar{\beta}}{m} \tanh\left(\frac{ma_{\tau 0}}{2}\right) = O(1) \quad (30)$$

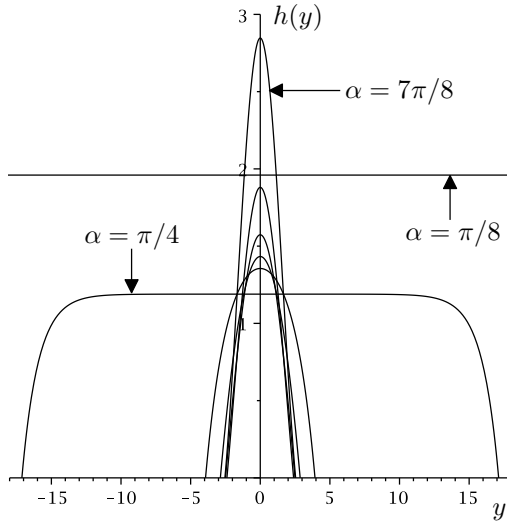


FIG. 8: Cross-sectional free surface profiles of the film H and the rivulet $h(y)$ when $\bar{\beta} = 1$, $\tau = -0.5$ and $\bar{Q} = 1$ at $\alpha = \pi/8$, $\pi/4$, $3\pi/8$, $\pi/2$, $5\pi/8$, $3\pi/4$, $7\pi/8$. Note that in this case $\pi/8 < \alpha_\infty \simeq 0.7112 < \pi/4$, and so the profile in the case $\alpha = \pi/8$ is that of an infinitely wide film of uniform thickness $H \simeq 1.9598$ rather than that of a finite-width rivulet.

on the upper half of the cylinder,

$$a \sim \left(\frac{105\bar{Q}}{4\bar{\beta}^3} \right)^{\frac{1}{4}} - \frac{7\tau}{8\bar{\beta}} \rightarrow \left(\frac{105\bar{Q}}{4\bar{\beta}^3} \right)^{\frac{1}{4}+} \quad \text{and} \quad h_m \sim \left(\frac{105\bar{Q}\bar{\beta}}{64} \right)^{\frac{1}{4}} - \frac{7\tau}{16} \rightarrow \left(\frac{105\bar{Q}\bar{\beta}}{64} \right)^{\frac{1}{4}+} \quad (31)$$

at $\alpha = \pi/2$, and according to (30) with “tanh” replaced by “tan” in the expression for h_m on the lower half of the cylinder, where $a_{\tau 0}$ is the semi-width in the special case of no shear, that is, the form of a when $\tau = 0$.

C. The Limit of Strong Shear ($\tau \rightarrow -\infty$)

In the limit of strong shear, $\tau \rightarrow -\infty$, $\alpha_\infty \rightarrow \pi/2^-$ according to (22) and the film becomes deep according to $H = -3\tau/(2\sin \alpha) \rightarrow \infty$ on the upper half of the cylinder, while the rivulet becomes wide and deep according to

$$a \sim -\frac{7\tau}{2\bar{\beta}} \rightarrow \infty \quad \text{and} \quad h_m \sim -\frac{7\tau}{4} \rightarrow \infty \quad (32)$$

at $\alpha = \pi/2$, and deep with finite width according to

$$a \sim \frac{\pi}{m} + \frac{10\bar{\beta}\sin \alpha}{9m^2\tau} \rightarrow \frac{\pi}{m} \quad \text{and} \quad h_m \sim -\frac{9\tau}{5\sin \alpha} \rightarrow \infty \quad (33)$$

on the lower half of the cylinder. Note that a changes from $O(\tau)$ to $O(1)$ in a narrow transition layer of width $O(\tau^{-2})$ near $\alpha = \pi/2^+$.

D. The Limit of Small Flux ($\bar{Q} \rightarrow 0^+$)

In the limit of small flux, $\bar{Q} \rightarrow 0^+$, the rivulet behaves according to

$$a \sim a_{Q0} + \frac{18m^3\bar{Q}}{\bar{\beta}^2 [2\bar{\beta} \sin \alpha f'(ma_{Q0}) + 9m\tau g'(ma_{Q0})]} \rightarrow a_{Q0}^+ \quad \text{and} \quad h_m \sim \frac{\bar{\beta}}{m} \tanh\left(\frac{ma_{Q0}}{2}\right) = O(1) \quad (34)$$

on the upper half of the cylinder for $\alpha_\infty < \alpha < \pi/2$,

$$a \sim -\frac{7\tau}{2\bar{\beta}} - \frac{30\bar{Q}}{49\tau^3} \rightarrow -\frac{7\tau^+}{2\bar{\beta}} \quad \text{and} \quad h_m \sim -\frac{7\tau}{4} - \frac{15\bar{\beta}\bar{Q}}{49\tau^3} \rightarrow -\frac{7\tau^+}{4} \quad (35)$$

at $\alpha = \pi/2$, and according to (34) with “tanh” replaced by “tan” in the expression for h_m on the lower half of the cylinder, where a_{Q0} is the semi-width in the special case of zero flux, that is, the form of a when $\bar{Q} = 0$.

E. The Limit of Large Flux ($\bar{Q} \rightarrow \infty$)

In the limit of large flux, $\bar{Q} \rightarrow \infty$, the rivulet becomes wide with finite thickness according to

$$a \sim \frac{3m^3\bar{Q}}{\bar{\beta}^2 [2\bar{\beta} \sin \alpha + 3m\tau]} \rightarrow \infty \quad \text{and} \quad h_m \sim \frac{\bar{\beta}}{m} \tanh\left(\frac{3m^4\bar{Q}}{2\bar{\beta}^2 [2\bar{\beta} \sin \alpha + 3m\tau]}\right) \rightarrow \frac{\bar{\beta}^-}{m} \quad (36)$$

on the upper half of the cylinder for $\alpha_\infty < \alpha < \pi/2$, wide and deep according to

$$a \sim \left(\frac{105\bar{Q}}{4\bar{\beta}^3}\right)^{\frac{1}{4}} - \frac{7\tau}{8\bar{\beta}} \rightarrow \infty \quad \text{and} \quad h_m \sim \left(\frac{105\bar{Q}\bar{\beta}}{64}\right)^{\frac{1}{4}} - \frac{7\tau}{16} \rightarrow \infty \quad (37)$$

at $\alpha = \pi/2$, and deep with finite width according to

$$a \sim \frac{\pi}{m} - \left(\frac{5\pi\bar{\beta}^3 \sin \alpha}{3m^7\bar{Q}}\right)^{\frac{1}{3}} \rightarrow \frac{\pi^-}{m} \quad \text{and} \quad h_m \sim \left(\frac{24\bar{Q}m}{5\pi \sin \alpha}\right)^{\frac{1}{3}} \rightarrow \infty \quad (38)$$

on the lower half of the cylinder; note that a and h_m in (38) are independent of τ to the orders given. Note also that a changes from $O(\bar{Q})$ to $O(1)$ and h_m changes from $O(1)$ to $O(\bar{Q}^{1/3})$ in a narrow transition layer of width $O(\bar{Q}^{-1/2})$ near $\alpha = \pi/2$.

V. A RIVULET WITH CONSTANT SEMI-WIDTH $a = \bar{a}$

In this section we describe the steady, locally unidirectional flow of a slowly varying rivulet with constant semi-width $a = \bar{a}$ but slowly varying contact angle $\beta = \beta(\alpha) (\geq 0)$ on

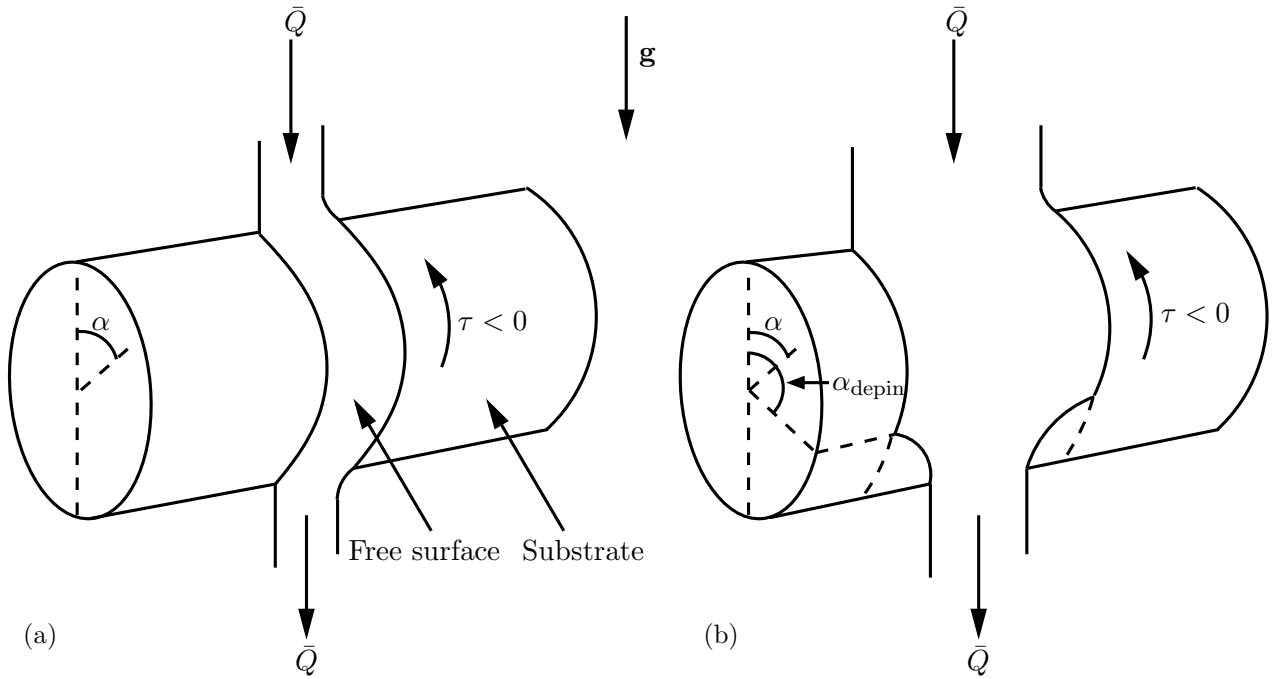


FIG. 9: Sketch of the scenario considered in Sec. V, namely a rivulet with prescribed flux \bar{Q} and (when not de-pinned with zero contact angle $\beta = \bar{\beta} = 0$ but slowly varying semi-width $a = \pi/m$) constant semi-width $a = \bar{a}$ but slowly varying contact angle β that runs from $\alpha = 0$ to $\alpha = \pi$, in the cases (a) $a = \bar{a} < \pi$, in which the rivulet is never de-pinned, and (b) $a = \bar{a} > \pi$, in which the rivulet is de-pinned and has zero contact angle in the interval $\alpha_{\text{depin}} \leq \alpha \leq \pi$.

the right-hand side of a large horizontal cylinder subject to a non-positive uniform azimuthal surface shear stress $\tau (\leq 0)$ acting in opposition to gravity.

Unlike in the case of constant non-zero contact angle described in Sec. IV in which the behaviour is qualitatively the same for all values of the contact angle, the behaviour is qualitatively different for a narrow rivulet with $a = \bar{a} < \pi$, in the marginal case $a = \bar{a} = \pi$, and for a wide rivulet with $a = \bar{a} > \pi$, and hence in Subsecs VA–VC we describe the behaviour in each of these three cases separately. In Subsec. VD we present examples of free surface profiles of the rivulet, and in Subsecs VE–VH we describe the behaviour in the limits of weak shear, $\tau \rightarrow 0^-$, strong shear, $\tau \rightarrow -\infty$, small flux, $\bar{Q} \rightarrow 0^+$, and large flux, $\bar{Q} \rightarrow \infty$, respectively.

A. A Narrow Rivulet with $a = \bar{a} < \pi$

For a narrow rivulet with $a = \bar{a} < \pi$ for all values of \bar{Q} and $\tau (\leq 0)$ there is a slowly varying rivulet that runs all the way from the top of the cylinder $\alpha = 0$ to the bottom

of the cylinder $\alpha = \pi$, and its contact angle β has a single minimum on the lower half of the cylinder and its maximum thickness h_m has a single minimum on the upper half of the cylinder. This scenario is sketched in Figure 9(a).

1. The Special Case of No Shear ($\tau = 0$)

In the special case of no shear, $\tau = 0$, the real positive solution of (7) for the contact angle β is

$$\beta = \left(\frac{9\bar{Q}m^4}{\sin \alpha f(m\bar{a})} \right)^{\frac{1}{3}}, \quad (39)$$

and the maximum thickness h_m is given by (6) with β given by (39). The rivulet becomes deep near the top and the bottom of the cylinder according to

$$\beta \sim \left(\frac{9\bar{Q}}{f(\bar{a})\alpha} \right)^{\frac{1}{3}} \rightarrow \infty \quad \text{and} \quad h_m \sim \left(\frac{9\bar{Q}}{f(\bar{a})\alpha} \right)^{\frac{1}{3}} \tanh\left(\frac{\bar{a}}{2}\right) \rightarrow \infty \quad (40)$$

as $\alpha \rightarrow 0^+$ and

$$\beta \sim \left(\frac{9\bar{Q}}{f(\bar{a})(\pi - \alpha)} \right)^{\frac{1}{3}} \rightarrow \infty \quad \text{and} \quad h_m \sim \left(\frac{9\bar{Q}}{f(\bar{a})(\pi - \alpha)} \right)^{\frac{1}{3}} \tan\left(\frac{\bar{a}}{2}\right) \rightarrow \infty \quad (41)$$

as $\alpha \rightarrow \pi^-$; also β and h_m take the $O(1)$ values

$$\beta = \left(\frac{105\bar{Q}}{4\bar{a}^4} \right)^{\frac{1}{3}} \quad \text{and} \quad h_m = \left(\frac{105\bar{Q}}{32\bar{a}} \right)^{\frac{1}{3}} \quad (42)$$

at $\alpha = \pi/2$. In the limit of a very narrow rivulet, $\bar{a} \rightarrow 0^+$, the rivulet becomes narrow and deep everywhere according to

$$\beta \sim \left(\frac{105\bar{Q}}{4\bar{a}^4 \sin \alpha} \right)^{\frac{1}{3}} \rightarrow \infty \quad \text{and} \quad h_m \sim \left(\frac{105\bar{Q}}{32\bar{a} \sin \alpha} \right)^{\frac{1}{3}} \rightarrow \infty. \quad (43)$$

2. The General Case of Strictly Negative Shear ($\tau < 0$)

In the general case of strictly negative shear, $\tau < 0$, the real positive solution of (7) for the contact angle β is

$$\beta = -\frac{3\tau m g(m\bar{a})}{2 \sin \alpha f(m\bar{a})} \left\{ 1 + 2 \cosh \left[\frac{1}{3} \cosh^{-1} \left(1 - \frac{4\bar{Q}m \sin^2 \alpha f^2(m\bar{a})}{3\tau^3 g^3(m\bar{a})} \right) \right] \right\}, \quad (44)$$

and the maximum thickness h_m is given by (6) with β given by (44). The rivulet becomes deep near the top and the bottom of the cylinder according to

$$\beta \sim -\frac{9\tau g(\bar{a})}{2\alpha f(\bar{a})} \rightarrow \infty \quad \text{and} \quad h_m \sim -\frac{9\tau g(\bar{a})}{2\alpha f(\bar{a})} \tanh\left(\frac{\bar{a}}{2}\right) \rightarrow \infty \quad (45)$$

as $\alpha \rightarrow 0^+$ and

$$\beta \sim -\frac{9\tau g(\bar{a})}{2(\pi - \alpha)f(\bar{a})} \rightarrow \infty \quad \text{and} \quad h_m \sim -\frac{9\tau g(\bar{a})}{2(\pi - \alpha)f(\bar{a})} \tan\left(\frac{\bar{a}}{2}\right) \rightarrow \infty \quad (46)$$

as $\alpha \rightarrow \pi^-$; also β and h_m take the $O(1)$ values

$$\beta = -\frac{7\tau}{6\bar{a}} \left\{ 1 + 2 \cosh \left[\frac{1}{3} \cosh^{-1} \left(1 - \frac{405\bar{Q}}{49\tau^3\bar{a}} \right) \right] \right\} \quad \text{and} \quad h_m = \frac{\beta\bar{a}}{2} \quad (47)$$

at $\alpha = \pi/2$. In the limit of a very narrow rivulet, $\bar{a} \rightarrow 0^+$, the rivulet becomes narrow and deep everywhere according to (43) (showing that, rather unexpectedly, its behaviour is independent of τ).

The behaviour of the present solution when $a = \bar{a} < \pi$ is illustrated in Figure 10, which shows plots of the contact angle β and the maximum thickness h_m as functions of α/π when $\bar{Q} = 1$ for (a,b) various values of $\tau (\leq 0)$ when $\bar{a} = 2 (< \pi)$ and for (c,d) various values of \bar{a} satisfying $\bar{a} < \pi$ when $\tau = -1$.

B. The Marginal Case $a = \bar{a} = \pi$

In the marginal case $a = \bar{a} = \pi$ the rivulet behaves qualitatively as in the case of a narrow rivulet with $a = \bar{a} < \pi$ except that, since in this case $\beta = 0$ at $\alpha = \pi$, instead of satisfying (41) in the special case of no shear, $\tau = 0$, or (46) in the general case of strictly negative shear, $\tau < 0$, the rivulet becomes deep with zero contact angle and finite semi-width π near the bottom of the cylinder according to

$$\beta \sim \left(\frac{3\pi^2\bar{Q}(\pi - \alpha)^5}{320} \right)^{\frac{1}{3}} \rightarrow 0^+ \quad \text{and} \quad h_m \sim \left(\frac{24\bar{Q}}{5\pi(\pi - \alpha)} \right)^{\frac{1}{3}} \rightarrow \infty \quad (48)$$

when $\tau = 0$ and

$$\beta \sim -\frac{9\pi\tau(\pi - \alpha)}{40} \rightarrow 0^+ \quad \text{and} \quad h_m \sim -\frac{9\tau}{5(\pi - \alpha)} \rightarrow \infty \quad (49)$$

when $\tau < 0$, as $\alpha \rightarrow \pi^-$.

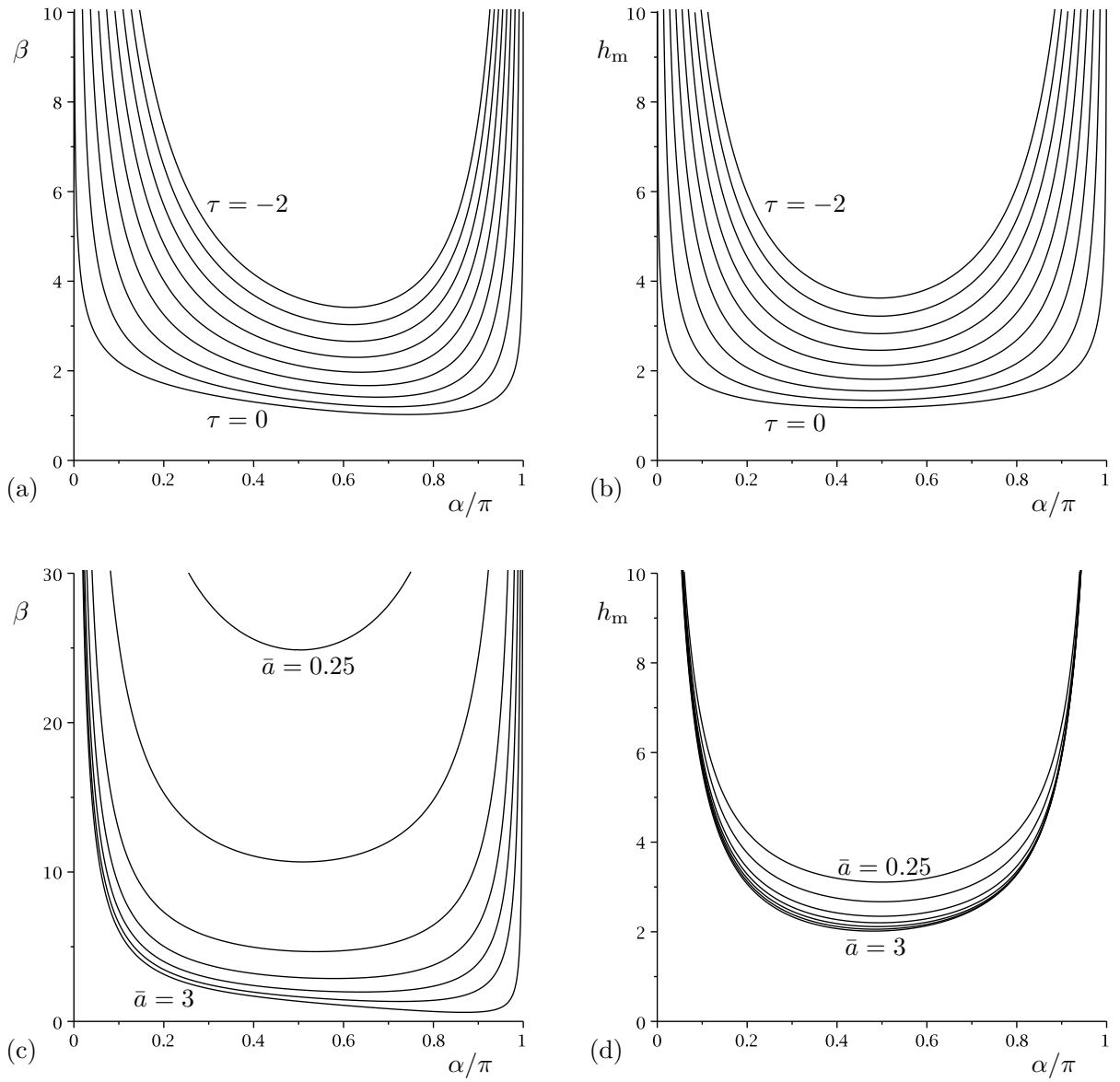


FIG. 10: Plots of (a,c) the contact angle β and (b,d) the maximum thickness h_m as functions of the scaled angle α/π when $\bar{Q} = 1$ for (a,b) $\tau = -2, -1.75, \dots, 0$ when $\bar{a} = 2 (< \pi)$, and (c,d) $\bar{a} = 0.25, 0.5, 1, \dots, 3$ when $\tau = -1$.

C. A Wide Rivulet with $a = \bar{a} > \pi$

Unlike for a narrow rivulet with $a = \bar{a} < \pi$, for a wide rivulet with $a = \bar{a} > \pi$ for all values of \bar{Q} and $\tau (\leq 0)$ there is a slowly varying rivulet that runs from the top of the cylinder $\alpha = 0$ only as far as a station $\alpha = \alpha_{\text{depin}}$ ($\pi/2 < \alpha_{\text{depin}} < \pi$) on the lower half of the cylinder, and its contact angle β , again given by (39) in the special case of no shear, $\tau = 0$, or (44) in the general case of strictly negative shear, $\tau < 0$, is a monotonically decreasing function of α , attaining its minimum physically realisable value of zero at the station $\alpha = \alpha_{\text{depin}}$, where

α_{depin} is given by

$$\alpha_{\text{depin}} = \cos^{-1} \left(-\frac{\pi^2}{\bar{a}^2} \right) \quad \text{for } \bar{a} > \pi. \quad (50)$$

Note that, rather unexpectedly, α_{depin} is independent of both τ and \bar{Q} , and hence coincides exactly with the corresponding angle found by Paterson, Wilson, and Duffy¹⁰ in the special case of no shear, $\tau = 0$. The rivulet again becomes deep near the top of the cylinder according to (40) when $\tau = 0$ or (45) when $\tau < 0$, and again β and h_m take the $O(1)$ values given by (42) when $\tau = 0$ or (47) when $\tau < 0$ at $\alpha = \pi/2$. At $\alpha = \alpha_{\text{depin}}$ the rivulet has zero contact angle $\beta = 0$, semi-width $a = \bar{a} > \pi$, and maximum thickness $h_m = h_{\text{mdepin}}$, where $h_{\text{mdepin}} (> 0)$ is the real positive solution of (16c) when $\alpha = \alpha_{\text{depin}}$, namely

$$h_{\text{mdepin}} = \left(\frac{24\bar{Q}\bar{a}}{5\sqrt{\bar{a}^4 - \pi^4}} \right)^{\frac{1}{3}} \quad (51)$$

when $\tau = 0$ and

$$h_{\text{mdepin}} = -\frac{3\tau\bar{a}^2}{5\sqrt{\bar{a}^4 - \pi^4}} \left\{ 1 + 2 \cosh \left[\frac{1}{3} \cosh^{-1} \left(1 - \frac{100\bar{Q}(\bar{a}^4 - \pi^4)}{9\tau^3\bar{a}^5} \right) \right] \right\} \quad (52)$$

when $\tau < 0$. Furthermore, as $\alpha \rightarrow \alpha_{\text{depin}}^-$ we find that $\beta \rightarrow 0^+$ according to

$$\beta = \beta_{\text{depin}} (\alpha_{\text{depin}} - \alpha) + O(\alpha_{\text{depin}} - \alpha)^2, \quad (53)$$

$a \equiv \bar{a}$, and $h_m \rightarrow h_{\text{mdepin}}^-$ according to

$$h_m = h_{\text{mdepin}} + \frac{5(\bar{a}^4 + \pi^4)h_{\text{mdepin}}^2 + 9\tau\bar{a}^2\sqrt{\bar{a}^4 - \pi^4}h_{\text{mdepin}}}{6\pi^2(5\sqrt{\bar{a}^4 - \pi^4}h_{\text{mdepin}} + 6\tau\bar{a}^2)} (\alpha - \alpha_{\text{depin}}) + O(\alpha - \alpha_{\text{depin}})^2, \quad (54)$$

where the coefficient $\beta_{\text{depin}} (> 0)$ in (53) is the real positive solution of the cubic polynomial equation that is obtained from (7) in the limit $\alpha \rightarrow \alpha_{\text{depin}}^-$, and is given by

$$\beta_{\text{depin}} = \frac{\sqrt{\bar{a}^4 - \pi^4}}{4\bar{a}} h_{\text{mdepin}}, \quad (55)$$

together with (51) or (52), as appropriate.

Since there is no physically realisable rivulet solution in the interval $\alpha_{\text{depin}} < \alpha \leq \pi$, an alternative description of the behaviour is required there. The scenario we will consider is the one proposed by Paterson, Wilson, and Duffy¹⁰, namely that for $0 \leq \alpha < \alpha_{\text{depin}}$ the rivulet behaves according to the description of a narrow rivulet given in Subsec. V A, but that the contact lines de-pin at $\alpha = \alpha_{\text{depin}}$, and the rivulet runs from $\alpha = \alpha_{\text{depin}}$ to the

bottom of the cylinder $\alpha = \pi$ with zero contact angle according to the solution in the case $\beta = \bar{\beta} = 0$ given by (16), with monotonically decreasing semi-width $a = \pi/m$ ($\pi \leq a \leq \bar{a}$) and monotonically increasing maximum thickness $h_m \geq h_{m\text{depin}}$. This scenario is sketched in Figure 9(b). In particular, as $\alpha \rightarrow \alpha_{\text{depin}}^+$ we find that $\beta \equiv 0$, $a \rightarrow \bar{a}^-$ according to

$$a \sim \bar{a} - \frac{\bar{a}\sqrt{\bar{a}^4 - \pi^4}}{2\pi^2}(\alpha - \alpha_{\text{depin}}) \rightarrow \bar{a}^-, \quad (56)$$

and $h_m \rightarrow h_{m\text{depin}}^+$ according to (54), so that the solutions in $\alpha < \alpha_{\text{depin}}$ and $\alpha > \alpha_{\text{depin}}$ join continuously (but not smoothly) at the station $\alpha = \alpha_{\text{depin}}$. Note that Paterson, Wilson, and Duffy¹⁰ considered the more general scenario of de-pinning and re-pinning at a non-zero contact angle, but for simplicity we restrict our attention to the simplest case of de-pinning at zero contact angle here.

1. The Special Case of No Shear ($\tau = 0$)

In the special case of no shear, $\tau = 0$, the real positive solution of (16c) for the maximum thickness h_m in the interval $\alpha_{\text{depin}} \leq \alpha \leq \pi$ is

$$h_m = \left(\frac{24\bar{Q}m}{5\pi \sin \alpha} \right)^{\frac{1}{3}}. \quad (57)$$

Near the bottom of the cylinder the rivulet becomes deep with finite semi-width π according to

$$a \sim \pi + \frac{\pi}{4}(\pi - \alpha)^2 \rightarrow \pi^+ \quad \text{and} \quad h_m \sim \left(\frac{24\bar{Q}}{5\pi(\pi - \alpha)} \right)^{\frac{1}{3}} \rightarrow \infty \quad (58)$$

as $\alpha \rightarrow \pi^-$. Also, in the limit of a very wide rivulet, $\bar{a} \rightarrow \infty$, for which $\alpha_{\text{depin}} \rightarrow \pi/2^+$, the rivulet becomes wide and flat according to

$$\beta \sim \left(\frac{3\bar{Q}m^3}{2\bar{a} \sin \alpha} \right)^{\frac{1}{3}} \rightarrow 0^+ \quad \text{and} \quad h_m \sim \left(\frac{3\bar{Q}}{2\bar{a} \sin \alpha} \right)^{\frac{1}{3}} \rightarrow 0^+ \quad (59)$$

on the upper half of the cylinder, and behaves according to the solution in the case $\beta = \bar{\beta} = 0$ given by (16) and (57) on the lower half of the cylinder.

2. The General Case of Strictly Negative Shear ($\tau < 0$)

In the general case of strictly negative shear, $\tau < 0$, the real positive solution of (16c) for the maximum thickness h_m in the interval $\alpha_{\text{depin}} \leq \alpha \leq \pi$ is

$$h_m = -\frac{3\tau}{5 \sin \alpha} \left\{ 1 + 2 \cosh \left[\frac{1}{3} \cosh^{-1} \left(1 - \frac{100Qm \sin^2 \alpha}{9\pi\tau^3} \right) \right] \right\}. \quad (60)$$

Near the bottom of the cylinder the rivulet has finite semi-width a that approaches the value π again according to (58) and becomes deep according to

$$h_m \sim -\frac{9\tau}{5(\pi - \alpha)} \rightarrow \infty \quad (61)$$

as $\alpha \rightarrow \pi^-$. At leading order in the limit of a very wide rivulet, $\bar{a} \rightarrow \infty$, for which $\alpha_{\text{depin}} \rightarrow \pi/2^+$, on the upper half of the cylinder β and h_m take the $O(1)$ forms

$$\beta = -\frac{3m\tau}{2 \sin \alpha} \quad \text{and} \quad h_m = -\frac{3\tau}{2 \sin \alpha} \quad (62)$$

and the rivulet behaves according to the solution in the case $\beta = \bar{\beta} = 0$ given by (16) and (60) on the lower half of the cylinder.

The behaviour of the present solution when $a = \bar{a} > \pi$ is illustrated in Figure 11, which shows plots of the contact angle β , the maximum thickness h_m and the semi-width a as functions of α/π when $\bar{Q} = 1$ for (a,b) various values of $\tau (\leq 0)$ when $\bar{a} = 5 (> \pi)$ and for (c,d) various values of \bar{a} satisfying $\bar{a} \geq \pi$ when $\tau = -1$.

D. Free Surface Profiles

Figure 12 shows examples of cross-sectional free surface profiles of the rivulet when $\tau = -1$ and $\bar{Q} = 1$ in the cases (a) $\bar{a} = 2 (< \pi)$ and (b) $\bar{a} = 5 (> \pi)$.

E. The Limit of Weak Shear ($\tau \rightarrow 0^-$)

In the limit of weak shear, $\tau \rightarrow 0^-$, β and h_m take the forms

$$\beta = \beta_0 + \tau\beta_1 + O(\tau^2) \quad \text{and} \quad h_m = h_{m0} + \tau h_{m1} + O(\tau^2). \quad (63)$$

The leading order terms β_0 and h_{m0} are the forms of the contact angle and maximum thickness in the special case of no shear, $\tau = 0$, given by (39) and (6), respectively, for

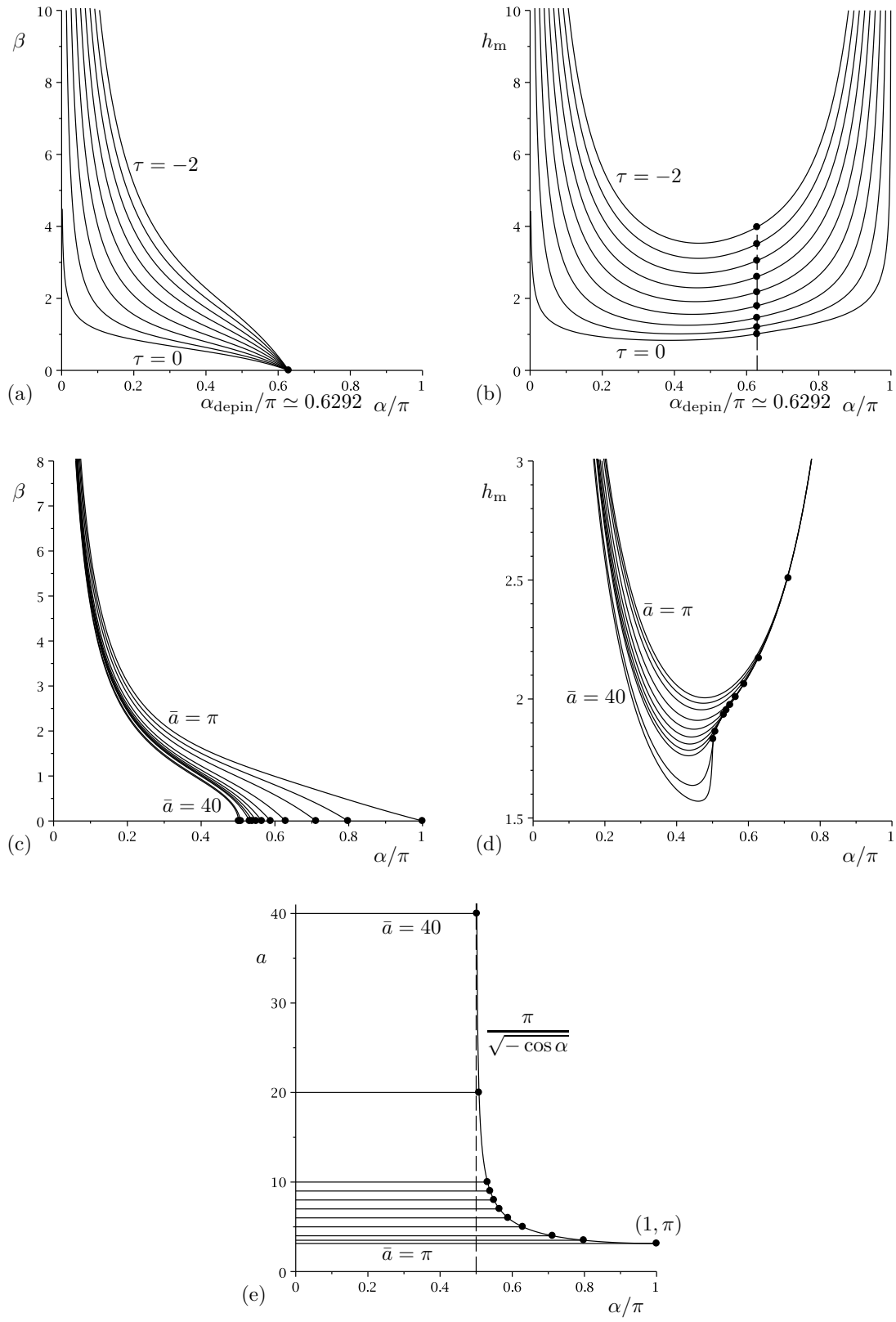


FIG. 11: Plots of (a,c) the contact angle β , (b,d) the maximum thickness h_m and (e) the semi-width a , all as functions of α/π ($0 \leq \alpha \leq \pi$) for (a,b) $\tau = -2, -1.75, \dots, 0$ when $\bar{a} = 5 (> \pi)$ and $\bar{Q} = 1$ and (c,d,e) $\bar{a} = \pi, 3.5, 4, 5, \dots, 10, 20, 40$ when $\tau = -1$ and $\bar{Q} = 1$. The dots indicate the corresponding values of $\alpha_{\text{depin}}/\pi$ given by (50) at which the contact lines de-pin.

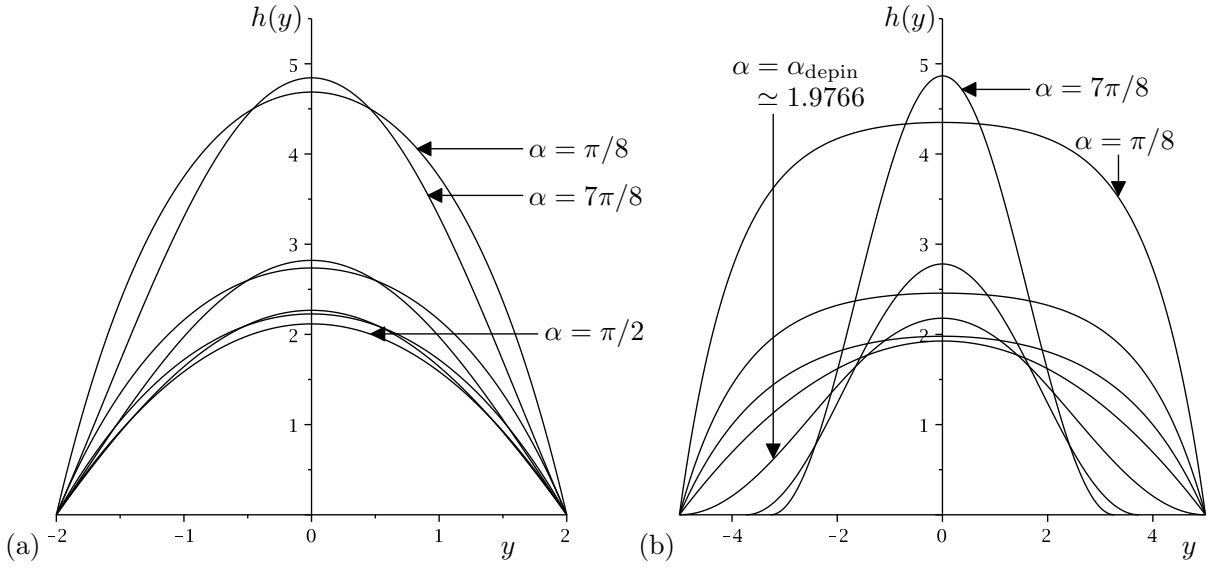


FIG. 12: Cross-sectional free surface profiles $h(y)$ when $\tau = -1$ and $\bar{Q} = 1$ in the cases (a) $\bar{a} = 2 (< \pi)$ at $\alpha = \pi/8, \pi/4, 3\pi/8, \pi/2, 5\pi/8, 3\pi/4, 7\pi/8$ and (b) $\bar{a} = 5 (> \pi)$ at $\alpha = \pi/8, \pi/4, 3\pi/8, \pi/2, \alpha_{\text{depin}} = \cos^{-1}(-\pi^2/25) \simeq 1.9766, 3\pi/4$ and $7\pi/8$. For clarity, the two parts of this figure use the same vertical but different horizontal ranges.

$0 \leq \alpha < \alpha_{\text{depin}}$, and by (57) on the lower half of the cylinder for $\alpha_{\text{depin}} \leq \alpha \leq \pi$. The first order terms β_1 and h_{m1} are given by

$$\beta_1 = -\frac{3mg(m\bar{a})}{2f(m\bar{a})\sin\alpha} \quad \text{and} \quad h_{m1} = -\frac{3g(m\bar{a})}{2f(m\bar{a})\sin\alpha} \tanh\left(\frac{m\bar{a}}{2}\right) \quad (64)$$

on the upper half of the cylinder,

$$\beta_1 = -\frac{7}{6\bar{a}} \quad \text{and} \quad h_{m1} = -\frac{7}{12} \quad (65)$$

at $\alpha = \pi/2$, (64) with “tanh” replaced by “tan” in the expression for h_{m1} on the lower half of the cylinder for $\pi/2 < \alpha < \alpha_{\text{depin}}$, and

$$h_{m1} = -\frac{3}{5\sin\alpha} \quad (66)$$

on the lower half of the cylinder for $\alpha_{\text{depin}} \leq \alpha \leq \pi$.

F. The Limit of Strong Shear ($\tau \rightarrow -\infty$)

In the limit of strong shear, $\tau \rightarrow -\infty$, the rivulet becomes deep according to

$$\beta \sim -\frac{9m\tau g(m\bar{a})}{2f(m\bar{a})\sin\alpha} \rightarrow \infty \quad \text{and} \quad h_m \sim -\frac{9\tau g(m\bar{a})}{2f(m\bar{a})\sin\alpha} \tanh\left(\frac{m\bar{a}}{2}\right) \rightarrow \infty \quad (67)$$

on the upper half of the cylinder,

$$\beta \sim -\frac{7\tau}{2\bar{a}} \rightarrow \infty \quad \text{and} \quad h_m \sim -\frac{7\tau}{4} \rightarrow \infty \quad (68)$$

at $\alpha = \pi/2$, (67) with “tanh” replaced by “tan” in the expression for h_m on the lower half of the cylinder for $\pi/2 < \alpha < \alpha_{\text{depin}}$, and

$$h_m \sim -\frac{9\tau}{5 \sin \alpha} \rightarrow \infty \quad (69)$$

on the lower half of the cylinder for $\alpha_{\text{depin}} \leq \alpha \leq \pi$. Note that β changes from $O(\tau)$ to zero in a narrow transition layer of width $O(\tau^{-1})$ near $\alpha = \alpha_{\text{depin}}^-$.

G. The Limit of Small Flux ($\bar{Q} \rightarrow 0^+$)

In the limit of small flux, $\bar{Q} \rightarrow 0^+$, the contact angle β behaves according to

$$\beta \sim \beta_{Q0} - \frac{2m^3\bar{Q}}{\beta_{Q0}\tau g(m\bar{a})} \rightarrow \beta_{Q0}^+, \quad (70)$$

and the maximum thickness h_m behaves according to (6) with β given by (70) for $0 \leq \alpha < \alpha_{\text{depin}}$, and

$$h_m \sim -\frac{9\tau}{5 \sin \alpha} + \frac{40m\bar{Q} \sin \alpha}{27\pi\tau^2} \rightarrow \left(-\frac{9\tau}{5 \sin \alpha}\right)^+ \quad (71)$$

on the lower half of the cylinder for $\alpha_{\text{depin}} \leq \alpha < \pi$, where β_{Q0} is the contact angle in the special case of zero flux, namely

$$\beta_{Q0} = -\frac{9m\tau g(m\bar{a})}{2 \sin \alpha f(m\bar{a})}. \quad (72)$$

H. The Limit of Large Flux ($\bar{Q} \rightarrow \infty$)

In the limit of large flux, $\bar{Q} \rightarrow \infty$, the contact angle and maximum thickness become large (i.e. $\beta \rightarrow \infty$ and $h_m \rightarrow \infty$, respectively) according to the solution in the special case of no shear, $\tau = 0$, given by (39) and (6) for $0 \leq \alpha < \alpha_{\text{depin}}$, and by (57) for $\alpha_{\text{depin}} \leq \alpha \leq \pi$. Note that β changes from $O(\bar{Q}^{1/3})$ to zero in a narrow transition layer of width $O(\bar{Q}^{-1/3})$ near $\alpha = \alpha_{\text{depin}}^-$.

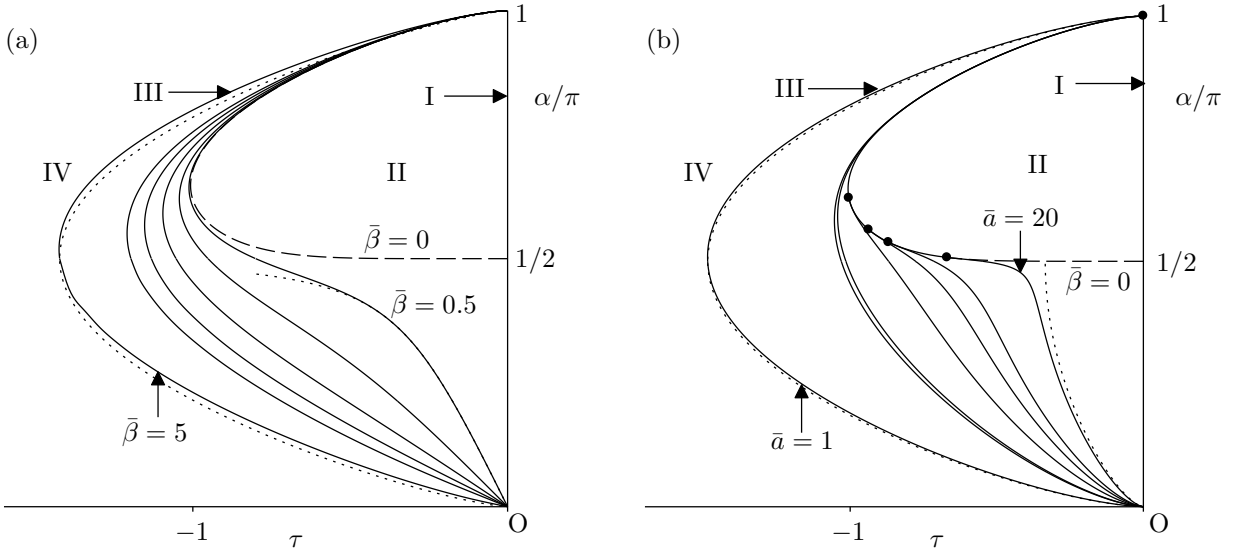


FIG. 13: Plots showing how the α/π - τ parameter plane is divided by curves corresponding to type-I and type-III flows into regions in which the solutions have the cross-sectional flow patterns of types I-IV described in Subsec. II D when $\bar{Q} = 1$ for (a) $\beta = \bar{\beta} = 0.5, 1, 1.5, 2, 2.5, 5$ and (b) $a = \bar{a} = 1, 3, \pi, 5, 7, 9, 20$. The dashed curves correspond to the special case of zero contact angle, $\beta = \bar{\beta} = 0$, given by (73), and in (b) the locations at which the curves corresponding to wide rivulets with $a = \bar{a} \geq \pi$ join this curve are marked with dots. The dotted curves show the solution in the limits of (a) small contact angle, $\bar{\beta} \rightarrow 0^+$, given by (74) for $0 \leq \alpha < \pi/2$ and plotted on the $\bar{\beta} = 0.5$ curve and large contact angle, $\bar{\beta} \rightarrow \infty$, given by (75) and plotted on the $\bar{\beta} = 5$ curve, and (b) a narrow rivulet, $\bar{a} \rightarrow 0^+$, given by (76) and plotted on the $\bar{a} = 1$ curve and a wide rivulet, $\bar{a} \rightarrow \infty$, given by (77) for $0 \leq \alpha < \pi/2$ and plotted on the $\bar{a} = 20$ curve.

VI. FLOW PATTERNS REVISITED

Figures 13(a) and 13(b) show how the α/π - τ parameter plane is divided by curves corresponding to type-I and type-III flows into regions in which the solutions have the cross-sectional flow patterns of types I-IV described in Subsec. II D when $\bar{Q} = 1$ (> 0) for rivulets with various constant contact angles $\beta = \bar{\beta}$ and various constant semi-widths $a = \bar{a}$, respectively. In particular, Figure 13 includes the curves corresponding to type-III flow in the special case of zero contact angle, $\beta = \bar{\beta} = 0$, namely

$$\tau = - \left(\frac{6\bar{Q}m \sin^2 \alpha}{\pi} \right)^{\frac{1}{3}}, \quad (73)$$

obtained using the fact that $h_m = -2\tau/\sin \alpha$ for type-III flow (as mentioned in Subsec. II D), together with (60). The maximum strength of (negative) shear such that type-III flow exists at some station $\alpha = \text{constant}$ on the cylinder is denoted by $\tau = \tau_{\text{III}m}$. As Figure 13 shows, there are two stations ($\alpha = \alpha_{\text{III}1}$ and $\alpha = \alpha_{\text{III}2} > \pi/2$, where $\alpha_{\text{III}1} < \alpha_{\text{III}2}$) at which type-III flow exists when $|\tau| < |\tau_{\text{III}m}|$, one ($\alpha = \alpha_{\text{III}} > \pi/2$) when $\tau = \tau_{\text{III}m}$, and none when

$|\tau| > |\tau_{\text{IIIIm}}|$. In the latter case the flow is always upwards at $z = h_m$ (i.e. type IV for all α). Of course, since $\bar{Q} > 0$, type-V flow is not possible here.

For type-III flow, in the limit of small contact angle, $\bar{\beta} \rightarrow 0^+$, we have

$$\tau \sim -\frac{\bar{\beta} \sin \alpha}{2m} \rightarrow 0^- \quad (74)$$

on the upper half of the cylinder and shown as a dotted curve in Figure 13(a) when $\bar{\beta} = 0.5$, and (73) on the lower half of the cylinder, shown as a dashed curve in Figure 13(a). In the limit of large contact angle, $\bar{\beta} \rightarrow \infty$, we have

$$\tau \sim -\frac{1}{4} (210\bar{Q}\bar{\beta} \sin^3 \alpha)^{\frac{1}{4}} \rightarrow -\infty, \quad (75)$$

shown as a dotted curve in Figure 13(a) when $\bar{\beta} = 5$. In the limit of a narrow rivulet, $\bar{a} \rightarrow 0^+$, we have

$$\tau \sim -\frac{1}{4} \left(\frac{210\bar{Q} \sin^2 \alpha}{\bar{a}} \right)^{\frac{1}{3}} \rightarrow -\infty, \quad (76)$$

shown as a dotted curve in Figure 13(b) when $\bar{a} = 1$. In the limit of a wide rivulet, $\bar{a} \rightarrow \infty$, we have

$$\tau \sim -\left(\frac{3\bar{Q} \sin^2 \alpha}{4\bar{a}} \right)^{\frac{1}{3}} \rightarrow 0^-, \quad (77)$$

on the upper half of the cylinder and shown as a dotted curve in Figure 13(b) when $\bar{a} = 20$, and (73) on the lower half of the cylinder, shown as a dashed curve in Figure 13(b).

Figure 14 shows sketches of the possible flow patterns within the film and the rivulet with constant non-zero contact angle described in Sec. IV in the vertical cross-section $y = 0$. In particular, Figures 14(a) and 14(b) show the case $|\tau| < |\tau_{\text{IIIIm}}|$, in which $\alpha_\infty < \alpha_{\text{III1}} < \pi/2$ and $\alpha_{\text{III1}} > \pi/2$, respectively, Figure 14(c) shows the case $\tau = \tau_{\text{IIIIm}}$, and Figure 14(d) shows the case $|\tau| > |\tau_{\text{IIIIm}}|$. Figure 14 also illustrates that the solutions for the film in $0 \leq \alpha \leq \alpha_\infty$ and for the rivulet in $\alpha_\infty < \alpha \leq \pi$ join continuously (but not smoothly) at the station $\alpha = \alpha_\infty$. The flow patterns within the rivulet with constant width described in Sec. V are rather similar to those shown in Figure 14 and hence are omitted for brevity.

VII. CONCLUSIONS

In the present work we investigated the flow of a slowly varying rivulet with positive prescribed flux $Q = \bar{Q} > 0$ on a slowly varying substrate, specifically the flow in the azimuthal

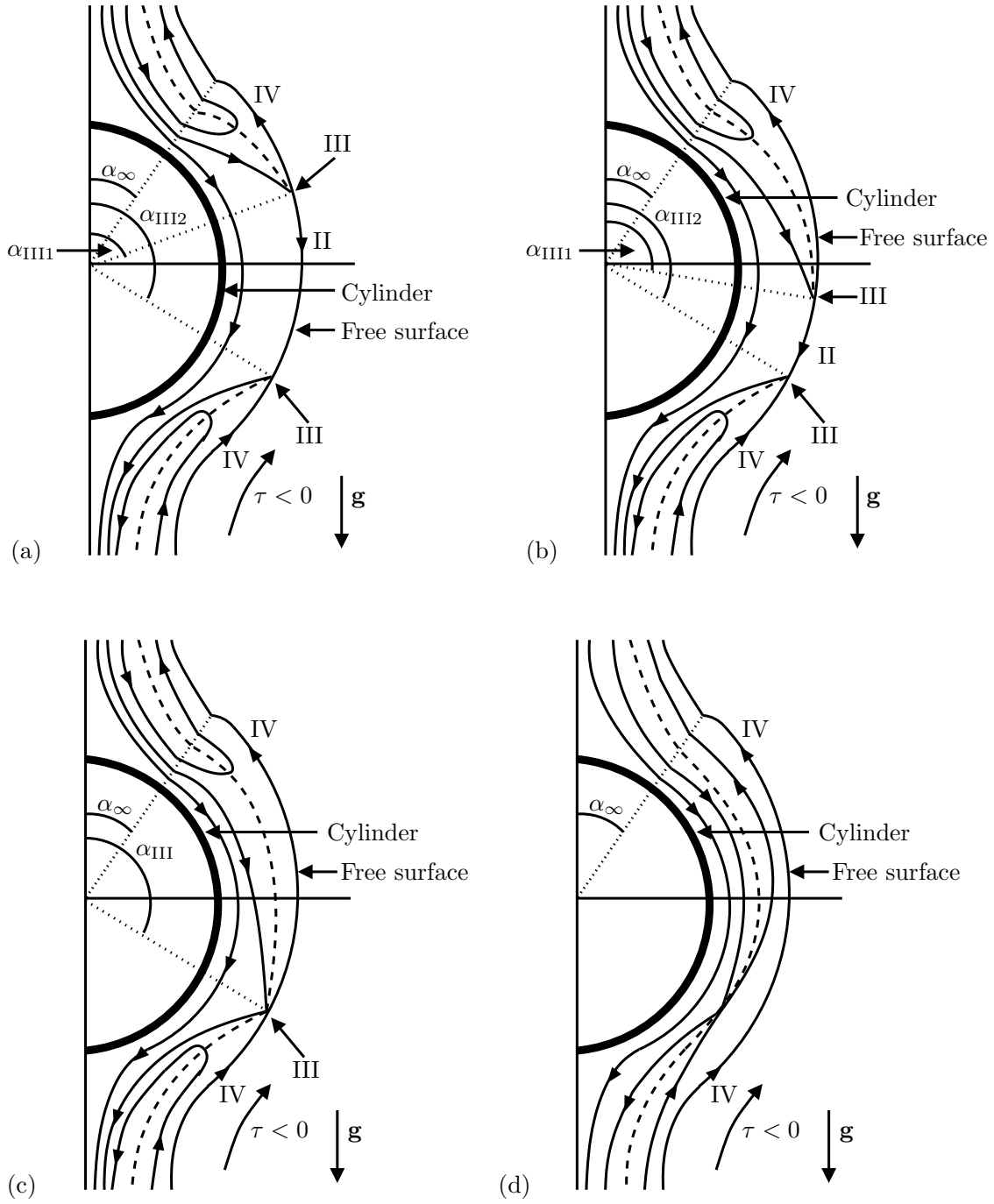


FIG. 14: Sketches of the possible flow patterns within the film and the rivulet in the vertical cross-section $y = 0$ when (a) $|\tau| < |\tau_{III\text{m}}|$ and $\alpha_{III1} < \pi/2$, (b) $|\tau| < |\tau_{III\text{m}}|$ and $\alpha_{III1} > \pi/2$, (c) $\tau = \tau_{III\text{m}}$, and (d) $|\tau| > |\tau_{III\text{m}}|$. The dashed curves indicate where $u = 0$.

direction round a large stationary horizontal cylinder, subject to a prescribed uniform azimuthal surface shear stress τ . In particular, we focused on the case of non-positive shear stress, $\tau \leq 0$, that is, opposing gravity, in which there is always a solution corresponding to a rivulet flowing down at least part of one side of the cylinder. We considered both a rivulet

with constant non-zero contact angle $\beta = \bar{\beta} > 0$ but slowly varying semi-width $a = a(\alpha)$ and a rivulet with constant semi-width $a = \bar{a}$ but slowly varying contact angle $\beta = \beta(\alpha)$, and showed that they have qualitatively different behaviour.

In Sec. IV we showed that, unlike in the special case of no shear, $\tau = 0$, considered by Duffy and Moffatt⁹, in the general case when shear is present, $\tau < 0$, a rivulet with constant non-zero contact angle $\beta = \bar{\beta} > 0$ can never run all the way from the top to the bottom of the cylinder, and so we considered the scenario sketched in Figure 6 in which an infinitely wide two-dimensional film of uniform thickness $H = -3\tau/(2 \sin \alpha) (> 0)$ covers the cylinder from the top $\alpha = 0$ to the station $\alpha = \alpha_\infty$, where it breaks into a single rivulet with constant non-zero contact angle but slowly varying width that runs from the station $\alpha = \alpha_\infty$ to the bottom $\alpha = \pi$. In particular, we showed that α_∞ is a monotonically increasing function of $-\tau$ which approaches the value $\pi/2$ from below in the limit $-\tau \rightarrow \infty$, and hence that as the strength of the (negative) shear increases the film covers an increasingly larger part of the upper half of the cylinder.

In Sec. V we showed that, like in the special case of no shear, $\tau = 0$, considered by Paterson, Wilson, and Duffy¹⁰, while a narrow rivulet with constant semi-width $a = \bar{a} \leq \pi$ can run all the way from the top $\alpha = 0$ to the bottom $\alpha = \pi$ of the cylinder, a wide rivulet with constant semi-width $a = \bar{a} > \pi$ can run from $\alpha = 0$ only to the station $\alpha = \alpha_{\text{depin}}$, where its contact angle becomes zero, and so we considered the scenario sketched in Figure 9 in which the contact lines de-pin at $\alpha = \alpha_{\text{depin}}$ and the rivulet flows from $\alpha = \alpha_{\text{depin}}$ to $\alpha = \pi$ with zero contact angle but slowly varying width. In particular, we showed that α_{depin} is independent of τ , and hence that as the strength of the shear is varied the rivulet always de-pins at the same station on the lower half of the cylinder.

As Figure 4 shows, the rivulet solutions described in the present work are not the only physically realisable solutions for flow on a stationary cylinder in the presence of a uniform azimuthal surface shear stress. In particular, as we described in Sec. III, full-ring solutions that extend all the way round the cylinder, which are impossible in the absence of shear, exist when the shear is sufficiently strong; these solutions will be analysed in a subsequent publication.

VIII. ACKNOWLEDGEMENTS

The first author (CP) gratefully acknowledges the financial support of the University of Strathclyde via a Postgraduate Research Scholarship. This work was begun while the second author (SKW) was a Visiting Fellow in the Oxford Centre for Collaborative Applied Mathematics (OCCAM), Mathematical Institute, University of Oxford, United Kingdom. This publication was based on work supported in part by Award No KUK-C1-013-04, made by King Abdullah University of Science and Technology (KAUST).

- ¹ G. Ribatski and A.M. Jacobi, Falling-film evaporation on horizontal tubes – a critical review. *Int. J. Refrig.* **28**, 635 (2005).
- ² P. Gorse, S. Busam, and K. Dullenkopf, Influence of operating condition and geometry on the oil film thickness in aeroengine bearing chambers. *J. Eng. Gas Turb. Power* **128**, 103 (2006).
- ³ M. Farrall, K. Simmons, S. Hibberd, and P. Gorse, A numerical model for oil film flow in an aeroengine bearing chamber and comparison to experimental data. *J. Eng. Gas Turb. Power* **128**, 111 (2006).
- ⁴ Y. Hikami and N. Shiraishi, Rain-wind induced vibrations of cables in cable-stayed bridges. *J. Wind Engng. Ind. Aerodyn.* **29**, 409 (1988).
- ⁵ A.C. Robertson, I.J. Taylor, S.K. Wilson, B.R. Duffy, and J.S. Sullivan, Numerical simulation of rivulet evolution on a horizontal cable subject to an external aerodynamic field. *J. Fluids and Structures* **26**, 50 (2010).
- ⁶ W. Nusselt, Die oberflächenkondensation des wasserdampfes. *Z. Vereines deutscher Ingenieure* **60**, 541 (1916).
- ⁷ W. Nusselt, Die oberflächenkondensation des wasserdampfes. *Z. Vereines deutscher Ingenieure* **60**, 569 (1916).
- ⁸ H.K. Moffatt, Behaviour of a viscous film on the outer surface of a rotating cylinder. *J. Méc.* **22**, 772 (1977).
- ⁹ B.R. Duffy and H.K. Moffatt, Flow of a viscous trickle on a slowly varying incline. *Chem. Eng. J.* **60**, 141 (1995).
- ¹⁰ C. Paterson, S.K. Wilson, and B.R. Duffy, Pinning, de-pinning and re-pinning of a slowly

- varying rivulet. to appear in Euro. J. Mech. B/Fluids (2013).
- ¹¹ G.A. Leslie, S.K. Wilson, and B.R. Duffy, Three-dimensional coating and rimming flow: a ring of fluid on a rotating horizontal cylinder. *J. Fluid Mech.* **716**, 51 (2013).
 - ¹² M. Villegas-Díaz, H. Power, and D.S. Riley, On the stability of rimming flows to two-dimensional disturbances. *Fluid Dyn. Res.* **33**, 141 (2003).
 - ¹³ M. Villegas-Díaz, H. Power, and D.S. Riley, Analytical and numerical studies of the stability of thin-film rimming flow subject to surface shear. *J. Fluid Mech.* **541**, 317 (2005).
 - ¹⁴ J.M. Sullivan, S.K. Wilson, and B.R. Duffy, A thin rivulet of perfectly wetting fluid subject to a longitudinal surface shear stress. *Q. J. Mech. Appl. Math.* **61**, 25 (2008).
 - ¹⁵ A.C. King, E.O. Tuck, and J.M. Vanden-Broeck, Air-blown waves on thin viscous sheets. *Phys. Fluids A* **5**, 973 (1993).
 - ¹⁶ F.-C. Chou and P.-Y. Wu, Effect of air shear on film planarization during spin coating. *J. Electrochem. Soc.* **147**, 699 (2000).
 - ¹⁷ S.K. Wilson, B.R. Duffy, and R. Hunt, A slender rivulet of a power-law fluid driven by either gravity or a constant shear stress at the free surface. *Q. J. Mech. Appl. Math.* **55**, 385 (2002).
 - ¹⁸ T.G. Myers and J.P.F. Charpin, A mathematical model for atmospheric ice accretion and water flow on a cold surface. *Int. J. Heat Mass Transf.* **47**, 5483 (2004).
 - ¹⁹ T.G. Myers, H.X. Liang, and B. Wetton, The stability and flow of a rivulet driven by interfacial shear and gravity. *Int. J. Nonlinear Mech.* **39**, 1239 (2004).
 - ²⁰ S.K. Wilson and B.R. Duffy, Unidirectional flow of a thin rivulet on a vertical substrate subject to a prescribed uniform shear stress at its free surface. *Phys. Fluids* **17**, 108105 (2005).
 - ²¹ N.H. Shuaib, H. Power, S. Hibberd, and K. Simmons, A numerical study of wave structures developed on the free surface of a film flowing on inclined planes and subjected to surface shear. *Int. J. Numer. Meth. Engng* **68**, 755 (2006).
 - ²² J.P. Pascal and S.J.D. D'Alessio, Instability of power-law fluid flows down an incline subjected to wind stress. *Appl. Math. Model.* **31**, 1229 (2007).
 - ²³ J.A. Cuminato, A.D. Fitt, M.J.S. Mphaka, and A. Nagamine, A singular integro-differential equation model for dryout in LMFBR boiler tubes. *IMA J. Appl. Math.* **75**, 269 (2010).
 - ²⁴ K. Ueno and M. Farzaneh, Linear stability analysis of ice growth under supercooled water film driven by a laminar airflow. *Phys. Fluids* **23**, 042103 (2011).
 - ²⁵ J.M. Sullivan, C. Paterson, S.K. Wilson, and B.R. Duffy, A thin rivulet or ridge subject to a

- uniform transverse shear stress at its free surface due to an external airflow. *Phys. Fluids* **24**, 082109 (2012).
- ²⁶ S. Luo, H. Li, W. Fei, and Y. Wang, Effect of counter current gas phase on liquid film. *Front. Chem. Eng. China* **3**, 135 (2009).
- ²⁷ S. Luo, H. Li, W. Fei, and Y. Wang, Liquid film characteristics on surface of structured packing. *Chinese J. Chem. Eng.* **17**, 47 (2009).

RECENT REPORTS

13/13	Pinning, de-pinning and re-pinning of a slowly varying rivulet	Paterson Wilson Duffy
13/14	Travelling-wave similarity solutions for a steadily translating slender dry patch in a thin fluid film	Yatim Duffy Wilson
13/15	A stochastic model for early placental development	Cotter Klika Kimpton Collins Heazell
13/16	Experimentally-calibrated population of models predicts and explains inter-subject variability in cardiac cellular electrophysiology	Britton Bueno-Orovio Van Ammel Lu Towart Gallacher Rodriguez
13/17	Elastometry of deflated capsules elastic moduli from shape and wrinkle analysis	Knoche Vella Aumaitre Degen Rehage Cicuta Kierfeld
13/18	The effect of a concentration-dependent viscosity on particle transport in a channel flow with porous walls	Herterich Griffiths Field Vella
13/19	On a poroviscoelastic model for cell crawling	Kimpton Whiteley Waters Oliver
13/20	Complexity Plots	Thiyagalingam Walton Duffy Trefethen Chen
13/21	Glyph-based video visualization for semen analysis	Duffy Thiyagalingam Walton Smith Trefethen Kirkman-Brown Gaffney Chen
13/22	RBF multiscale collocation for second order elliptic boundary value problems	Farrell Wendland

13/28	Minimizing synchronizations in sparse iterative solvers for distributed supercomputers	Zhu Gu Liu
13/29	Computational probabilistic quantification of pro-arrhythmic risk from scar and left-to-right heterogeneity in the human ventricles	Wallman Bueno-Orovio Rodriguez
13/30	Population of human ventricular cell models calibrated with in vivo measurements unravels ionic mechanisms of cardiac alternans	Zhou Bueno-Orovio Orini Hanson Haywood Taggart Lambiase Burrage Rodriguez
13/31	On the eigenvalues and eigenvectors of nonsymmetric saddle point matrices preconditioned by block triangular matrices	Pestana
13/32	Singular inextensible limit in the vibrations of post-buckled rods: analytical derivation and role of boundary conditions	Neukirch Goriely Thomas
13/33	Interfacial deflection and jetting of a paramagnetic particle-laden fluid: theory and experiment	Tsai Griffiths Li Kim Stone
13/34	A lattice Boltzmann model for natural convection in cavities	Allen Reis
13/35	Fractional diffusion models of cardiac electrical propagation : role of structural heterogeneity in dispersion of repolarization	Bueno-Orovio Kay Grau Rodriguez Burrage

Copies of these, and any other OCCAM reports can be obtained from:

**Oxford Centre for Collaborative Applied Mathematics
Mathematical Institute
24 - 29 St Giles'
Oxford
OX1 3LB
England
www.maths.ox.ac.uk/occam**